iScience

CellPress

Article

Toll-Interacting Protein Regulates Immune Cell Infiltration and Promotes Colitis-Associated Cancer

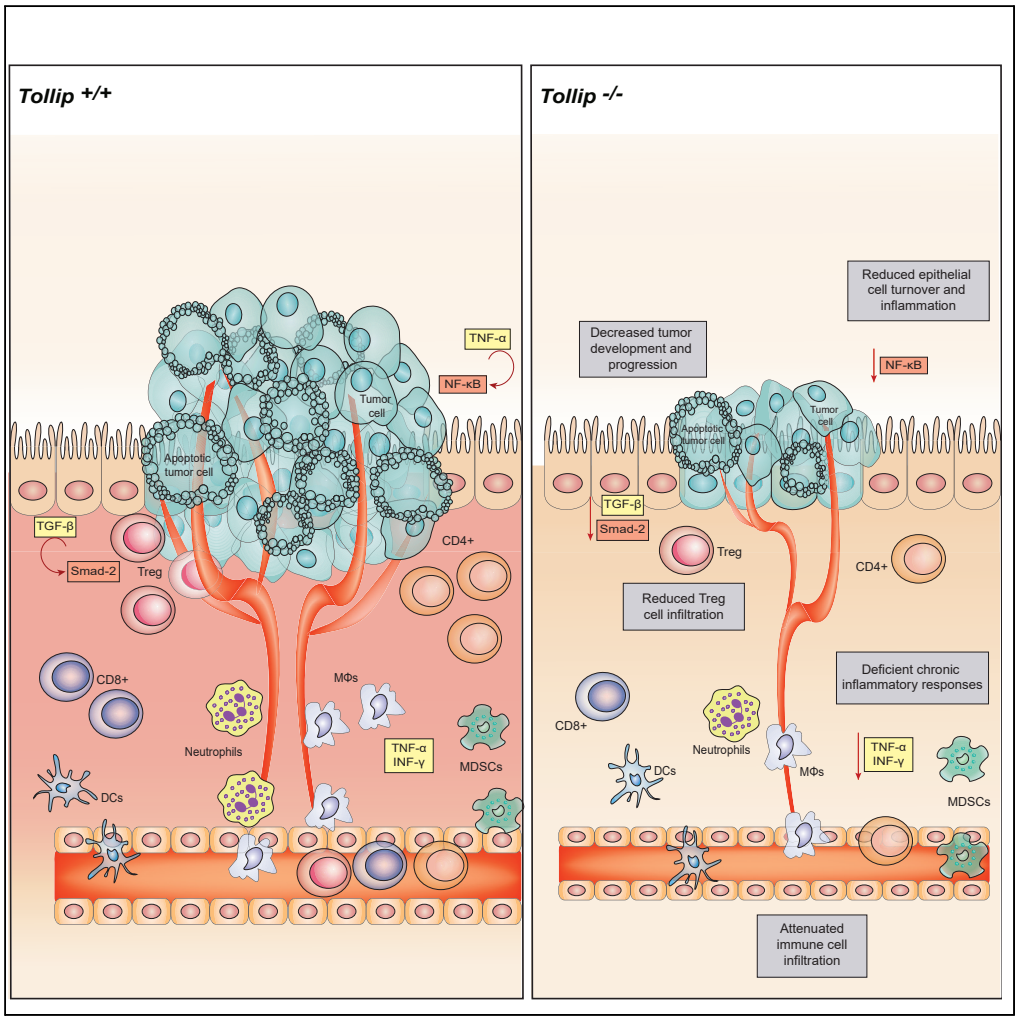

Christina Begka, Céline Pattaroni, Catherine Mooser, Stéphane Nancey, Kathy D. McCoy, Dominique Velin, Michel H. Maillard

michel.maillard@chuv.ch

HIGHLIGHTS

Tollip protects from colitis but promotes colitis-associated cancer onset

Tollip-deficient tumors demonstrate decreased cell turnover and inflammation

Tollip ablation favors naive CD8$^+$ T cell accumulation in peripheral lymphoid organs

Regulatory T cell accumulation is aberrant in Tollip-deficient tumors

Begka et al., iScience *23*, 100891
March 27, 2020
https://doi.org/10.1016/j.isci.2020.100891

iScience

CellPress

Article

Toll-Interacting Protein Regulates Immune Cell Infiltration and Promotes Colitis-Associated Cancer

Christina Begka,[1,2] Céline Pattaroni,[3] Catherine Mooser,[4] Stéphane Nancey,[5] Swiss IBD Cohort Study Group,[8] Kathy D. McCoy,[4,6] Dominique Velin,[1,2] and Michel H. Maillard[1,2,7,9,*]

SUMMARY

Expression of Toll-interacting protein (Tollip), a potent TLR modulator, decreases in patients with inflammatory bowel diseases (IBD), whereas Tollip$^{-/-}$ mice are susceptible to colitis. *Tollip* expression was shown to be reduced in sporadic adenoma . In contrast, we found variable *Tollip* expression in patients with colitis-associated adenomas. In Tollip$^{-/-}$ mice challenged to develop colitis-associated cancer (CAC), tumor formation was significantly reduced owing to decreased mucosal proliferative and apoptotic indexes. This protection was associated with blunt inflammatory responses without significant changes in microbial composition. mRNA expression of *Cd62l* and *Ccr5* homing receptors was reduced in colons of untreated Tollip$^{-/-}$ mice, whereas CD62L^{+} CD8^{+} T cells accumulated in the periphery. In Tollip-deficient adenomas *Ctla-4* mRNA expression and tumor-infiltrating CD4^{+} Foxp3^{+} regulatory T cell (Treg) were decreased. Our data show that protection from CAC in Tollip-deficient mice is associated with defects in lymphocyte accumulation and composition in colitis-associated adenomas.

INTRODUCTION

Patients with inflammatory bowel diseases (IBD) with long-standing and extensive colitis are at higher risk of developing a distinct type of colorectal cancer, termed colitis-associated cancer (CAC) (Canavan et al., 2006; Rutter et al., 2004). Although CAC etiology is complex and still incompletely understood, compromised epithelial integrity and deregulated Toll-like receptors (TLRs)-mediated microbiota sensing are important risk factors (Danese and Mantovani, 2010). Disruption of this microbiota sensing mechanism either at the receptor level or via downstream adaptor molecules, such as Myd88 ablation, results in increased production of pro-inflammatory cytokines and colitis development (Rakoff-Nahoum et al., 2004), favoring CAC onset (Lowe et al., 2010; Salcedo et al., 2010).

Dysbiosis and abundance of specific microbiota members can also influence carcinogenesis. Genomic analysis of human CRC biopsies detected a high prevalence of bacterial species such as *Fusobacterium nucleatum* and *Bacteroides fragilis* and have the ability to aggravate tumor propensity in mice (Kostic et al., 2012; Toprak et al., 2006). Consistently, blocking of TLR/MyD88-mediated sensing abrogated colorectal carcinogenesis (Rakoff-Nahoum and Medzhitov, 2007).

Regulation of NF-κB activity is essential to avoid spontaneous and prolonged inflammatory responses upon receptor binding. In mice lacking IκB kinase β (IKKβ), CAC susceptibility (Greten et al., 2004) was attributed to enhanced NF-κB-mediated IL-6 production and activation of STAT3-dependent epithelial neoplastic changes (Bollrath et al., 2009). Similarly, ablation of TLR4 or chemokine receptor signals results in impaired immune cell infiltration and protection of mice against CAC (Popivanova et al., 2009; Katoh et al., 2013; Fukata et al., 2007). Consistently, lack of negative regulators of innate immune signals, such as A20, single immunoglobulin receptor related molecule (SIGIRR), and interleukin receptor associated kinase-M (IRAK-M), was shown to enhance susceptibility to CAC in both humans and mice (Shao et al., 2013; Xiao et al., 2007; Kesselring et al., 2016; Begka et al., 2016). In CAC, although epithelial changes are essential to promote colon cancer, immune cell recruitment into the inflamed mucosa fuels tumor growth through perpetuation of inflammation (Greten et al., 2004). Regulatory T cells (Tregs) control intestinal inflammation, but their contribution in colorectal carcinogenesis remains elusive and controversial (Whiteside, 2012; Ladoire et al., 2011).

[1]Service of Gastroenterology and Hepatology, Department of Medicine, University Hospital of Lausanne, CHUV-Lausanne, Rue du Bugnon 46, 1011 Lausanne, Switzerland

[2]University of Lausanne, Chemin des Boveresses 155, 1066 Epalinges, Switzerland

[3]Service of Pneumology, Department of Medicine, Centre Hospitalier Universitaire Vaudois, University of Lausanne, Chemin de Boveresses 155, 1066 Epalinges, Switzerland

[4]Maurice Müller Laboratories (DBMR), Universitätsklinik für Viszerale Chirurgie und Medizin Inselspital, University of Bern, Murtenstrasse 35, 3010 Bern, Switzerland

[5]Lyon Sud Hospital, Hospices Civils de Lyon, CHU, Lyon, France

[6]Department of Physiology and Pharmacology, Cumming School of Medicine, University of Calgary, Calgary, AB T2N 4N1, Canada

[7]Crohn and Colitis Center, Gastroentérologie Beaulieu SA, Lausanne, Switzerland

[8]See "consortia section" for detailed list of authors

[9]Lead Contact

*Correspondence: michel.maillard@chuv.ch

https://doi.org/10.1016/j.isci.2020.100891

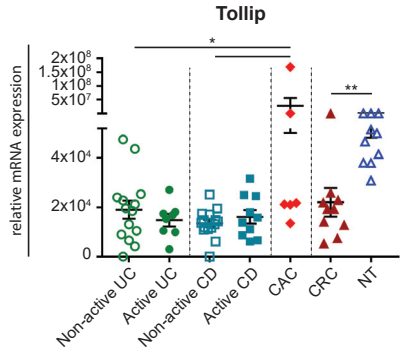

Figure 1. Tollip Expression in Biopsies from Patients with IBD and Colon Cancer

qRT-PCR analysis of *Tollip* mRNA expression relative to *Gapdh* in active and inactive gut segments from patients with UC and CD. n = 14 and n = 8 for UC and n = 15 and n = 10 for CD, respectively. Tollip expression was also assessed in biopsies from adenomas developed in patients with IBD (CAC, n = 6) and sporadic colorectal cancer (CRC, n = 10). As control, RNA extracts from the non-tumoral colon adjacent to the CRC (n = 10) were taken. Data are mean ± SEM. Differences were analyzed by one-way ANOVA test for CAC versus non-active UC and CAC versus non-active CD; $p = 0.0497$ and $p = 0.0458$, were calculated, respectively. Differences between CRC and NT were analyzed by Wilcoxon matched-pairs test, $p = 0.0020$. *$p < 0.05$, **$p < 0.01$.

Toll-interacting protein (Tollip) is an intracellular, ubiquitously expressed adaptor protein, initially described as a negative regulator of NF-κB signaling (Burns et al., 2000; Bulut et al., 2001). Upon activation of IL-1R, TLR2, and TLR4, Tollip recruits interleukin receptor associated kinase 1 (IRAK1) but inhibits its disassociation, depending on the stimulus strength, thus resulting in discontinuation of NF-κB pathway (Bulut et al., 2001; Burns et al., 2000; Zhang and Ghosh, 2002; Begka et al., 2016). Tollip also regulates the turnover of ubiquitinated receptors, such as IL-1R and TGFβ-RI, through clathrin-mediated endosomal trafficking and sorting to late endosomes (Brissoni et al., 2006; Zhu et al., 2012; Begka et al., 2016).

We have previously shown that Tollip deficiency increases susceptibility of mice to a dextran sodium sulfate (DSS) colitis model (Maillard et al., 2014). Tollip ablation resulted in disruption of tight junctions and increased intestinal permeability upon acute DSS chemical injury, whereas non-hematopoietic expression of Tollip partially restored disease susceptibility (Maillard et al., 2014). Tollip has also been linked to human IBD as its gene lies within one of the IBD susceptibility loci (van Heel et al., 2004; Ishihara et al., 2009). In addition, Tollip expression was downregulated in biopsies from both active and inactive colonic segments from patients with ulcerative colitis (UC) and Crohn's disease (CD) compared with healthy subjects (Fernandes et al., 2016).

Despite the demonstrated role of Tollip in colitis, its influence on inflammation-associated cancer remains unknown. In this study, we report that Tollip promotes colitis-driven carcinogenesis. We found that Tollip-deficient mice fail to mount efficient chronic inflammatory responses resulting in reduced tumor risk. Those global defects were also accompanied by qualitative changes in cellular composition with a reduction in tumor-infiltrating regulatory T cells.

RESULTS

Variable *Tollip* mRNA Expression in Patients with CAC

Although Tollip expression is decreased in sporadic colorectal cancer (CRC) adenomas (Pimentel-Nunes et al., 2012), there are no data available for human colitis-associated cancer (CAC) lesions. Given the link between inflammation and inflammation-driven cancer, we hypothesized that Tollip should be downregulated in CAC lesions. Therefore, we investigated *Tollip* mRNA expression in patients with IBD with active or quiescent UC or CD, as well as in CAC or sporadic CRC adenomas, compared with adjacent non-tumorous (NT) mucosal biopsies from sporadic CRC. Consistent with previous reports, we observed reduced *Tollip* mRNA expression in mucosa of patients with quiescent and active UC and CD compared with the control NT mucosal biopsies (Figure 1). Moreover, *Tollip* expression was downregulated in paired mucosal samples of sporadic CRC adenomas compared with NT normal adjacent mucosa (Figure 1). Surprisingly, *Tollip* expression in patients with CAC was variable and not significantly decreased, as we initially hypothesized.

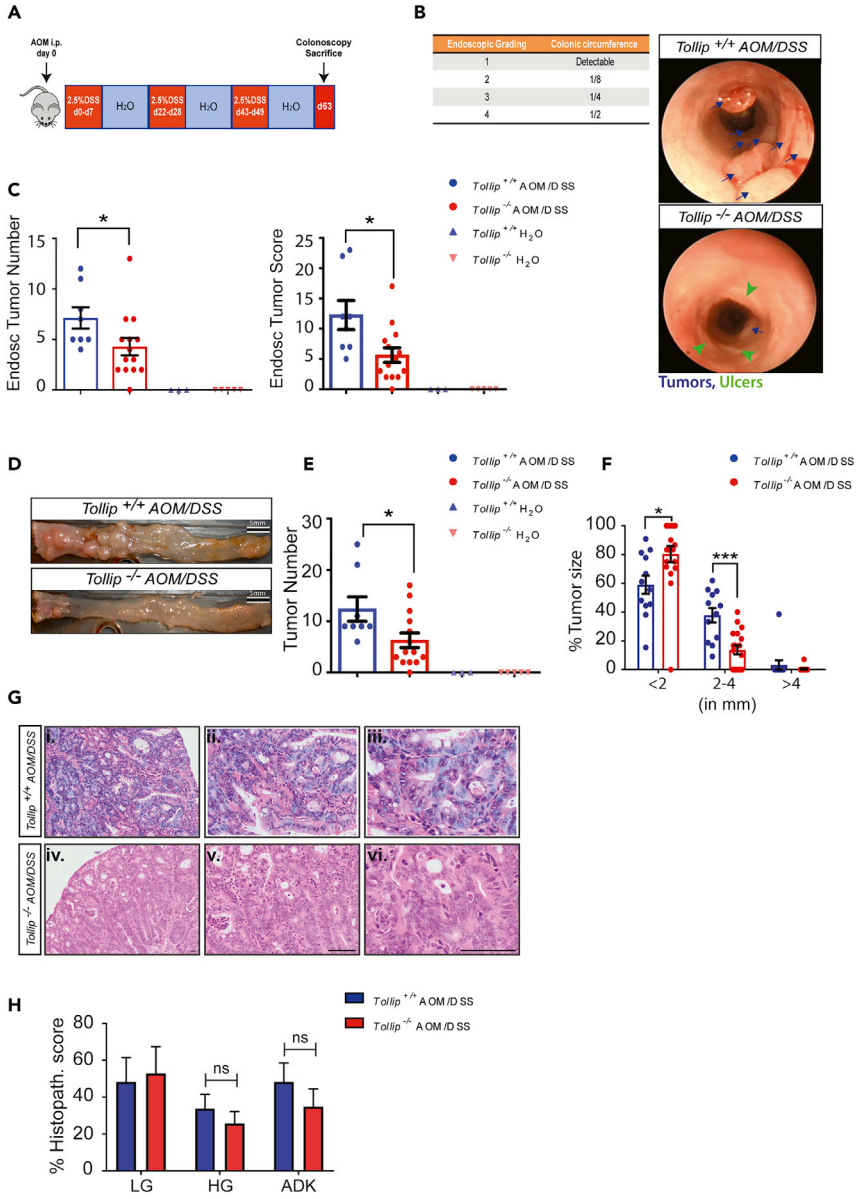

Figure 2. Tollip Deficiency Attenuates Colitis-Associated Carcinogenesis

(A) Tollip$^{-/-}$ and WT littermates C57BL/6 mice received a single intraperitoneal AOM injection (10 mg/kg) followed by three cycles of 2.5% DSS in drinking water. Unchallenged Tollip$^{-/-}$ and WT littermates were used as controls. On day 63, mice were subjected to colonoscopy to assess adenoma development and size.

(B) An endoscopic score was determined according to a standardized grading system (Becker et al., 2005). Representative endoscopic images from AOM/DSS exposed WT (upper panel) and Tollip$^{-/-}$ littermates at day 63. Tumors are depicted with blue arrows and ulcer formation with green arrowheads.

(C) Endoscopic tumor number and score in AOM/DSS-exposed WT and Tollip$^{-/-}$ littermates and unchallenged animals. Each dot represents data from an individual mouse. Data are mean ± SEM; n = 3–5 for unchallenged and n = 8–14 for treated groups. Differences were analyzed by Mann-Whitney test. p = 0.0318, p = 0.0106, for tumor number and score, respectively.

(D) Macroscopic evaluation of adenomatous lesions in excised colons from treated Tollip$^{-/-}$ and WT littermates.

(E and F) Quantification of overall macroscopic tumor number and size in AOM/DSS exposed Tollip$^{-/-}$ and WT littermates. Data are mean ± SEM; n = 8–14. Differences were analyzed by Mann-Whitney test, p = 0.0299 for macroscopic tumor number. Differences were analyzed with multiple t tests for macroscopic tumor size; p = 0.02 and p = 0.0001 for <2 and 2–4 mm, respectively.

Figure 2. *Continued*

(G) Histological evaluation of tubular adenomas formation by hematoxylin and eosin staining (H&E) in paraffin-embedded colons of Tollip WT (i–iii) and Tollip$^{-/-}$ treated mice **(iv–vi)** in increasing magnifications of 10×, 20×, and 40×. Scale bars: 100 μm.

(H) Histopathological score of adenomas in H&E staining of paraffin-embedded colons, LG, low-grade dysplasia; HG, high-grade dysplasia; ADK, adenocarcinoma. Differences were analyzed by two-tailed unpaired t test. Data are mean ± SEM. n = 8–19. ns $p > 0.5$, *$p < 0.05$, ***$p < 0.001$.

Tollip expression was higher in 2/6 CAC samples, histologically characterized as adenocarcinoma, compared with 4/6 CAC samples of low-grade dysplastic lesions, as well as with patients with quiescent and active UC and CD, whereas it was comparable with NT normal adjacent mucosa biopsies (Figure 1). In summary, Tollip expression is differentially regulated in CAC lesions compared with sporadic adenomas. We decided to further investigate the role of Tollip in an *in vivo* mouse model of chronic colitis-associated cancer onset, in which adenomas do not develop a differential dysplastic grade.

Tollip Ablation Is Protective against Colitis-Associated Cancer

To decipher the role of Tollip in CAC and avoid the variability introduced by human biopsies, we employed a CAC model in mice lacking Tollip expression. Tollip$^{-/-}$ and wild-type (WT) littermates were challenged with the azoxymethanone (AOM)/dextran sodium sulfate (DSS) model to recapitulate CAC development (Figure 2A). Adenoma growth and development were monitored by mouse colonoscopy at day 63 (Figures 2A and 2B). We observed significantly fewer adenomas and reduced endoscopic tumor scores (Becker et al., 2005) in the AOM/DSS-exposed Tollip$^{-/-}$ compared with WT mice, indicating that Tollip ablation resulted not only in reduced tumor incidence but also in smaller lesions (Figures 2B and 2C). Consistently, macroscopic examination of the excised colons demonstrated reduced tumor number upon Tollip ablation (Figures 2D and 2E). We also observed a significant increase in small (<2 mm) lesions and decrease in larger (2–4 mm) lesions in Tollip$^{-/-}$ compared with WT mice (Figure 2F), indicating that Tollip ablation results in the formation of smaller adenomas, in accordance with the observed endoscopic score (Figure 2C). Histological analyses confirmed the development of adenomatous AOM/DSS-induced polyps (Figure 2G), whereas frequency of dysplastic low-high grade or adenocarcinoma development was similar between Tollip$^{-/-}$ and WT mice (Figure 2H). These data, together with our previous findings, suggest that Tollip has a dual role in favoring CAC development despite being protective against acute colitis.

Tollip Deficiency Is Associated with Reduced Cell Turnover in Colonic Adenomas

Given the protective role of Tollip in colonic epithelium during acute inflammation (Maillard et al., 2014), we hypothesized that reduced tumor incidence in Tollip$^{-/-}$ mice could be related to defects in cell turnover rates. To address this hypothesis, we assessed apoptosis during tumor initiation and late tumor stage in the CAC model. At the beginning of AOM/DSS treatment (day 8) we observed a significant increase in epithelial apoptotic Tunel^{+} cells in Tollip-deficient colons (Figures 3A and 3B). However, at late tumor stage (day 63) the apoptotic index was significantly decreased in both Tollip-deficient adenomas (Figures 3C and 3E) and crypts of adjacent non-adenomatous mucosa of Tollip$^{-/-}$-treated animals compared with WT-treated mice (Figures 3D and 3F). Notably, the density of apoptotic cells was higher at the tip of colonic crypts in acute inflammation/early stage carcinogenesis on day 8 (Figure 3A), whereas analysis of late-stage carcinogenesis on day 63 showed a shift toward the lamina propria (Figure 3D). The apoptotic index was similar in unchallenged mice (Figure 3F) and our multi-screen gene analysis showed a downregulation of additional apoptosis-related genes in Tollip-deficient adenomas compared with WT (Figure S1A). We also observed a significantly reduced proliferative index in Tollip-deficient compared with WT adenomas (Figure 3G). We next examined STAT-3 activation (Figures S1B–S1D), along with important upstream and downstream targets involved with neoplastic properties of the STAT3 pathway (Figure S1E). Immunohistochemical analyses of the active form of STAT3 (P-STAT3) (Figure S1B) and relative P-STAT3 expression levels, although variable, were comparable between Tollip$^{-/-}$ and WT adenomas (Figures S1C and S1D) and in colons of untreated animals (Figure S1D). Similarly, *Bcl-xL*, *c-myc*, *Bax*, *IL-6*, and *IL-11* mRNA expression was comparable between Tollip$^{-/-}$ and WT adenomas (Figure S1E). In unchallenged Tollip$^{-/-}$ mice, *Bcl-xL* and *c-myc* mRNA expression was lower in whole colon homogenates compared with WT mice, indicating that the mucosal environment upon homeostatic conditions tends to be skewed toward a pro-apoptotic response (Figure S1E). However, this was not correlated with an impaired STAT3 signaling during tumorigenesis as both total and P-STAT3 protein abundance were comparable in Tollip$^{-/-}$ and WT adenomas, as well as in unchallenged mucosa (Figures S1B–S1D). Taken together, these results indicate

that Tollip deficiency induces pronounced epithelial apoptosis upon early tumorigenesis but, in the late tumor stage, Tollip deficiency results in retarded development and progress of adenomas with low turnover rates.

Reduced Cancer Risk in Tollip-Deficient Animals Is Not Associated with Changes in Gut Microbial Composition

Given the role of Tollip as regulator of the Toll/IL-1R signaling and the implication of several of those pathways in microbiota shaping, we hypothesized that changes in gut microbial composition might account for reduced cancer occurrence in Tollip-deficient mice. We performed 16S rRNA amplicon sequencing on feces of co-housed Tollip$^{-/-}$ and WT littermates prior and after AOM/DSS treatment. There was no difference in microbiota diversity between the two groups both at baseline (Figure S2A) and after treatment (Figure S2B). As inflammation-induced colon tumorigenesis has been linked with shifts in microbiota composition, we next addressed differences in microbiota composition between Tollip$^{-/-}$ and WT littermates. There were no differences in overall microbiota composition both before (ANOSIM p = 0.474) (Figure S2C) and following AOM/DSS treatment (ANOSIM, p = 0.5083, Figure S2D). The relative abundance of bacterial taxa at the phylum level was comparable between Tollip$^{-/-}$ and WT mice both before and after treatment (Figure S2E). Finally, we evaluated changes in specific bacterial taxonomic groups using differential abundance testing. We detected a minor enrichment of unclassified genus of *Peptococcaceae* (p = 0.019, LDA score = 1.5326) in WT mice and *Rikenellaceae* family of also unclassified genera and of unclassified families within the *Bacteroidales* order (p = 0.028) in stools of Tollip$^{-/-}$ mice (p = 0.034, LDA score = 2.1055 and 2.0850) (Figure S2F) following AOM/DSS treatment. Finally, AOM/DSS treatment itself led to a decrease in families within the *Proteobacteria* phylum, independently of genotype (Figure S2G). Altogether, these data demonstrate that reduced tumor incidence upon Tollip deficiency does not correlate with a tumor-protective shift in microbiota diversity or global composition.

Tollip Modulates Migration Patterns and Cell Infiltration in Colonic Mucosa

We next aimed to investigate whether Tollip ablation could influence mucosal immune inflammation-related cell composition. Multi-gene RNA screening in healthy colons of unchallenged animals demonstrated a significant reduction in L-selectin (*Cd62L*) mRNA expression (Figure 4A), an adhesion molecule known to regulate trafficking of naive or central memory T (T_N or T_{CM}) cells from blood to secondary lymphoid organs (Masopust and Schenkel, 2013). We also observed a non-significant reduction in several T cell homing markers such as *Cd44*, *Il7r*, and *Ccr7*, as well as the integrins *Itgβ2* and *Itgα4* that form the heterodimers LFA-1 and the gut-homing α4β7 (Masopust and Schenkel, 2013), respectively (Table S1). Next, we assessed whether T cell recruitment to the healthy gut mucosa was influenced by Tollip ablation under basal conditions. We found no differences in the CD3$^+$/CD4$^+$/CD8$^+$ T cell abundance in the colons of unchallenged mice (Figure 4B). However, investigation of the activation status of Tollip-deficient T cells in the periphery demonstrated a significant increase in the percentage of CD8$^+$ CD44$^-$ CD62L$^+$ T_N (naive) cells in spleen, blood, and peripheral lymph nodes (pLNs) (Figures 4C and 4D). The percentages of CD8$^+$ CD44^{hi} CD62L$^-$ T effector (T_{eff}) (Figures 4C and 4D) and CD4$^+$ CD44$^-$ CD62L$^+$ T_N and CD4$^+$ CD44^{hi} CD62L$^-$ T_{eff} cell were comparable between Tollip$^{-/-}$ and WT mice (Figures S3A and S3B). Interestingly, we also observed a significant reduction in *Ccr5* mRNA expression in Tollip$^{-/-}$ mice (Figure 4A, Table S1), a chemokine receptor known to mediate the recruitment of immune cells upon inflammatory conditions (Griffith et al., 2014). Collectively, these results suggest that Tollip deficiency favors naive cell accumulation in peripheral lymphoid organs upon homeostatic conditions.

Tollip Deficiency Impedes Infiltration of CD4+ and Regulatory T Cells in Adenomas

We next questioned whether the altered cell trafficking noted upon Tollip ablation during homeostatic conditions would impede immune cell accumulation and attenuate inflammatory responses upon AOM/DSS challenge. Despite Tollip commonly being described as a negative regulator (Zhang and Ghosh, 2002), several pro-inflammatory genes were downregulated in Tollip-deficient compared with WT adenomas (Figure S4A). Investigation of other inflammatory indexes, such as colonic shortening, was moderate in treated Tollip$^{-/-}$ mice compared with the significantly reduced colon length observed in WT mice (Figure S4B). We also noticed a significant reduction in CD45$^+$ cells frequency and absolute number infiltrates in Tollip-deficient adenomas compared with WT (Figure S4C). In addition, we also observed a prominent reduction of IFNγ- and TNFα-producing inflammatory cells infiltration into colons of challenged Tollip$^{-/-}$ mice compared with WT mice (Figure S4D). Collectively, these data suggest that Tollip aggravates

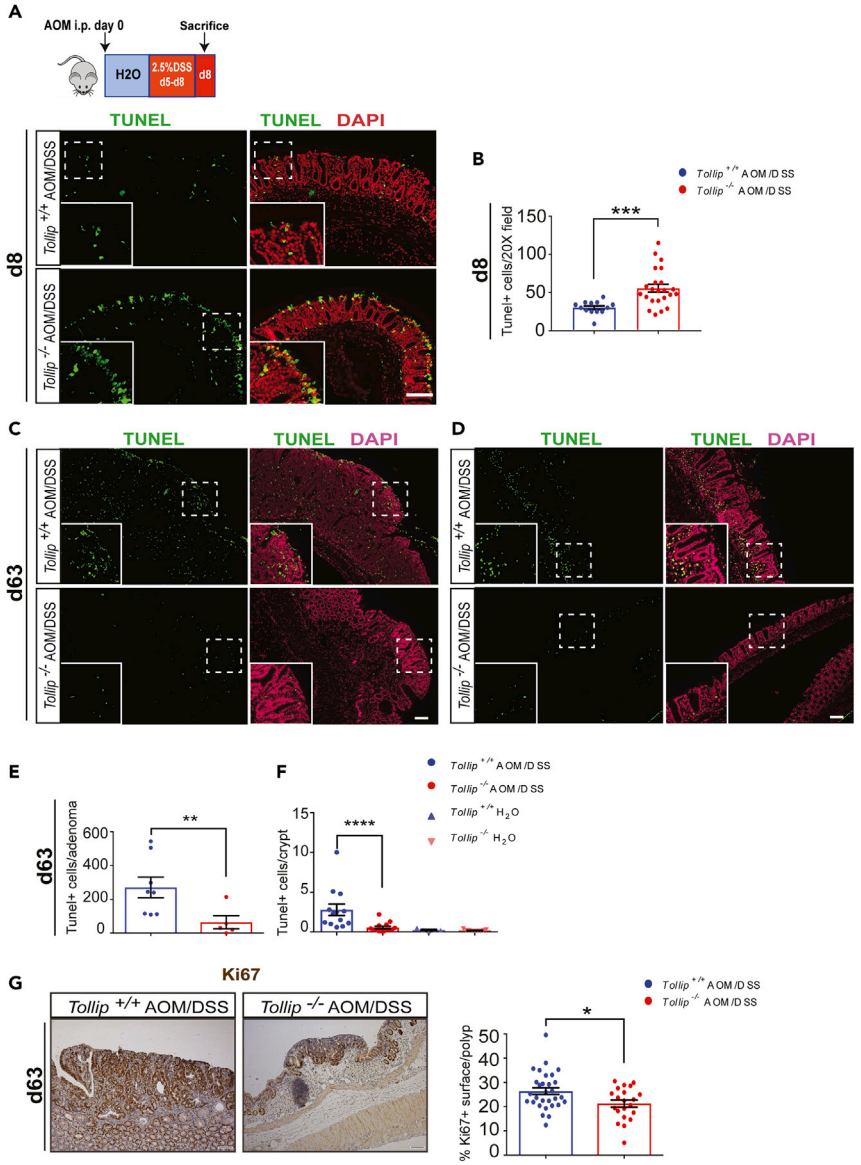

Figure 3. Tollip-Deficient Adenomas Present Reduced Proliferative and Apoptotic Indexes

(A) Tollip$^{-/-}$ and WT C57BL/6 littermates received a single i.p. AOM injection (10 mg/kg). After 5 days mice received oral treatment of 2.5% DSS in the drinking water and were euthanized on day 8; n = 5–6 mice. Cells apoptosis was quantified via immunofluorescent analysis of TUNEL^{+} cells on day 8. DAPI was used for nuclear staining. Scale bars: 100 μm. Insets show a magnified view of the TUNEL^{+} apoptotic cells.

(B) Quantification of TUNEL^{+} apoptotic cells in 20× field for at least three representative pictures/mouse. Data are mean ± SEM. Differences were evaluated with Mann-Whitney test. p = 0.0001.

(C and D) (C) Immunofluorescent evaluation of apoptosis by TUNEL staining in adenomas and (D) normal adjacent mucosa of AOM/DSS-exposed mice. DAPI was used for nuclear staining. Scale bars: 100 μm. Insets show a magnified view of the TUNEL^{+} apoptotic cells.

(E and F) (E) Quantification of TUNEL^{+} apoptotic cells in adenomas and (F) normal adjacent mucosa of treated as well as in colons of untreated mice in 10× field view for at least three representative pictures per mouse. Data are mean ± SEM. n = 5–14. Differences were analyzed by Mann-Whitney test. p = 0.0059 and p < 0.0001 for adenomas and normal mucosa crypts, respectively.

(G) Representative immunohistochemical Ki67 and nuclear staining with hematoxylin in adenomas of paraffin-embedded colons from AOM/DSS-treated mice. Scale bars: 100 μm. Analysis of proliferative index by measuring the percentage of surface of Ki67/nuclear staining ratio specifically for the adenomas by ImageJ algorithm Immunoratio. Counting was performed in 10× field view for at least three representative pictures/adenoma. Data are mean ± SEM. n = 5–7 mice and n = 21–34 adenomas. Differences were analyzed by Mann-Whitney test, p = 0.0357. **p < 0.01, ***p < 0.001, and ****p < 0.0001.

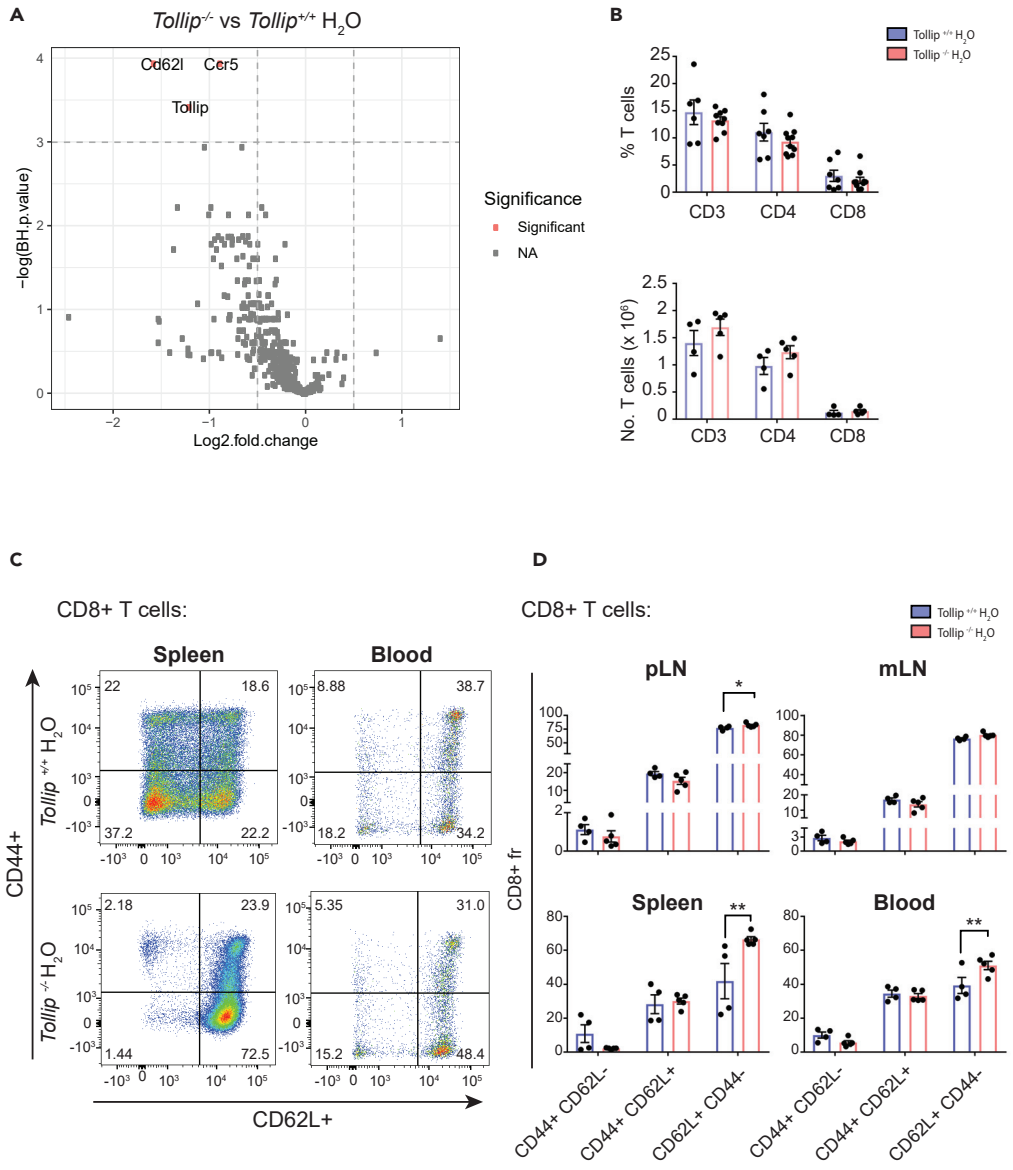

Figure 4. Tollip Deficiency Alters Migration Patterns upon Homeostatic Conditions

(A) Volcano plot depicts differential gene expression in colonic mucosa of untreated Tollip$^{-/-}$ and WT littermates (data obtained from three biological replicates per group).

(B) Flow cytometry analysis of colonic lamina propria T cells frequency and absolute cell numbers in untreated Tollip$^{-/-}$ and WT littermates. Data are mean ± SEM. n = 5–7 mice.

(C) Representative FACS plots of CD44^{+} and CD62L^{+} T cells frequencies in spleen and blood, pre-gated on CD8^{+} T lymphocytes.

(D) Flow cytometry analysis of naive and effector CD8^{+} T cells frequencies isolated from peripheral (pLN) and mesenteric (mLN) lymph nodes, spleen, and blood. Data are mean ± SEM; n = 4–5 mice. Differences were analyzed by one-way ANOVA test. p = 0.045, p = 0.0031, and p = 0.0015 values were calculated for pLN, spleen, and blood, respectively. *p < 0.05, **p < 0.01.

inflammatory responses at late tumor stage development (day 63), whereas no differences in CD45^{+} frequency and infiltration were observed in pLNs, mLNs, ileum, and spleen (Figure S5A).

Given our observation of reduced immune cell infiltration in Tollip$^{-/-}$ adenomas (Figure S4C), we further questioned whether reduced CD45^{+} cell accumulation was associated with defects in CD3^{+} T cell

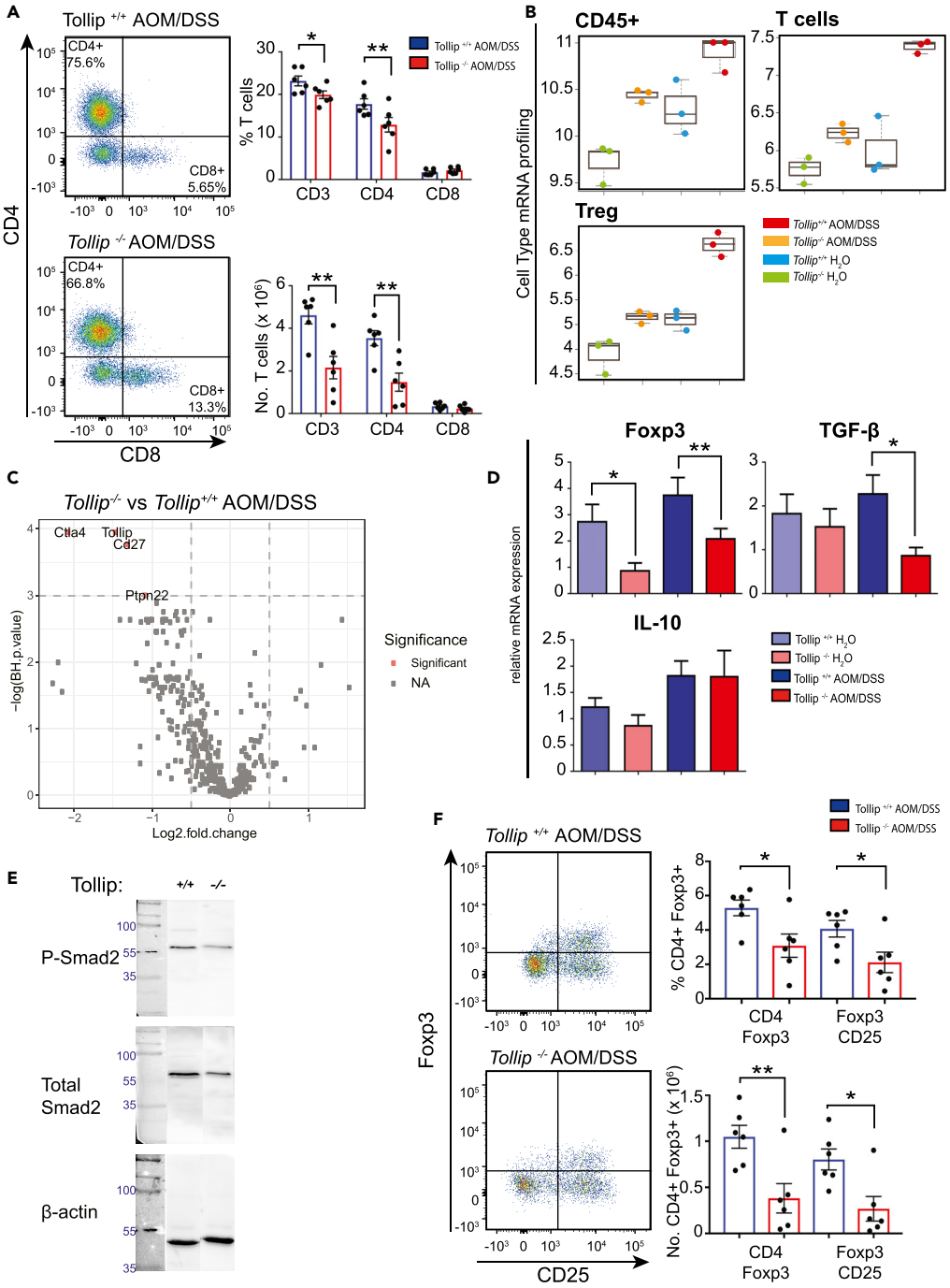

Figure 5. Tollip Deficiency Impairs T Regulatory Cells Accumulation into Colitis-Associated Adenomas

(A) Representative FACS plots of tumor-infiltrating T cells and analysis of $CD3^+$, $CD4^+$, and $CD8^+$ T cells frequencies and absolute cell numbers isolated from adenomas of $Tollip^{-/-}$ and WT mice. Data are mean ± SEM; n = 6 mice. Differences were analyzed by multiple t test. p = 0.03 and p = 0.003 values were calculated for $CD3^+$ and $CD4^+$ T cell frequencies, and p = 0.004 and p = 0.004 values were calculated for $CD3^+$ and $CD4^+$ T absolute cells numbers, respectively.

(B) Cell type mRNA profiling scores for $CD45^+$, T cells, and T regulatory (Treg) cells are calculated for adenomas and colon mucosa of treated and untreated $Tollip^{-/-}$ and WT mice.

(C) Volcano plot depicts differential gene expression in adenomas of AOM/DSS-exposed $Tollip^{-/-}$ versus WT littermates (data obtained from three biological replicates per group).

Figure 5. *Continued*

(D) Relative mRNA expression of *Foxp3*, *TGF-β*, and *IL-10* analyzed by real-time PCR. *Gadph* was used as a house keeping gene. Data are mean ± SEM; n = 5–19 samples. Differences were analyzed by two-tailed unpaired t test. p = 0.0228 for colons of untreated mice and p = 0.0027 *Foxp3* values for adenomas were calculated and p = 0.0317 for *TGF-β* for adenomas.

(E) Immunoblot analysis for phosphorylated Smad-2 (P-Smad-2, band at 60kD) and total Smad-2 (band at 60kD) protein extracted from whole colon homogenates from tumors (T) of both treated mice. β-Actin (at 42 kD) was used as a loading control. The pre-stained protein ladder appears before the protein bands of interest. The molecular bands of 100, 55, and 35 kD are noted in the pre-stained protein ladder that appears before the protein bands of interest. The same nitrocellulose membrane was used for the immunoblotting of all three markers.

(F) Representative FACS plots of tumor-infiltrating $CD4^+$ $CD25^+$ $Foxp3^+$ T regulatory cells and analysis of $CD4^+$ $Foxp3^+$ and $CD4^+$ $CD25^+$ $Foxp3^+$ Treg cells frequencies and absolute numbers isolated from adenomas of $Tollip^{-/-}$ and WT mice. Data are mean ± SEM; n = 6 mice. Differences were analyzed by t test. p = 0.023 and p = 0.0041 values were calculated for Treg frequencies and absolute cell numbers, respectively. *p < 0.05, **p < 0.01.

infiltration. As expected, we observed a marked colon-specific decrease in the frequency and number of $CD3^+$ T cell infiltrates in $Tollip^{-/-}$ compared with WT adenomas (Figure 5A). This decrease was mainly due to reductions in $CD4^+$ T cells frequency and infiltrates (Figure 5A). Importantly, this defect was only seen in the colonic adenomas but not in peripheral lymphoid organs (Figure S5B), suggesting that the observed changes are restricted to the mucosal environment during carcinogenesis.

To further investigate this reduced colon-specific infiltration of inflammatory cells, we performed a multi-screen RNA analysis. In line with the flow cytometry data (Figure S4C), a lower $CD45^+$ mRNA cell score was predicted for the challenged $Tollip^{-/-}$ compared with WT mice (Figure 5B), indicative of attenuated inflammatory responses. *Tollip* expression was used as internal control and was, as expected, not expressed in Tollip-deficient samples (Figure 5C). We observed a non-significant trend of reduced expression of genes relevant to the immune cells homing to inflammatory sites in colons of treated $Tollip^{-/-}$ versus WT mice (Table S2). Additionally, we found a significant reduction in expression of three key T cell receptor signaling-associated genes in Tollip-deficient adenomas (Tanoue et al., 2016; Hill et al., 2002; van de Ven and Borst, 2015), namely, *Ctla4*, *Cd27*, and *Ptpn22* (Figure 5C, Table S2).

Ctla4 is a costimulatory molecule that prevents excessive T cell activation upon TCR ligation. It has also been shown to be constitutively expressed on regulatory T cells (Sansom, 2000). Given the observed reduction in *Ctla4* expression in Tollip-deficient adenoma, we hypothesized that defects in immunosuppressive pathways could be observed upon Tollip ablation. Indeed, cell type mRNA profiling suggested reduced T lymphocytes and regulatory T cell abundance in both whole colon homogenates of unchallenged and adenomas of AOM/DSS-challenged $Tollip^{-/-}$ mice (Figure 5B). Accordingly, we noted a significant reduction in *Foxp3* mRNA expression in both healthy mucosa and adenomas of $Tollip^{-/-}$ compared with WT mice (Figure 5D). Furthermore, *TGF-β* but not *Il10* mRNA expression was downregulated in Tollip-deficient adenomas (Figure 5D). Consistently, we found a significant decrease in phospho-Smad2 and total Smad2 protein abundance that are known downstream effectors of *TGF-β* (Figure 5E). Altogether, those data demonstrate that Tollip ablation leads to reduced immunoregulatory T cell accumulation and blunted TGF-β/TGFβR-mediated responses.

Finally, we sought to determine the Treg frequencies and cell numbers systemically (Figure S5C) and in adenomas (Figure 5F). Indeed, we wanted to examine whether reduced $CD3^+$ T cell accumulation in adenomas was also associated with an imbalance between effector and regulatory T cells. In association with our prior results, we detected reduced $CD4^+$ $Foxp3^+$ and CD4+ $Foxp3^+$ $CD25^+$ frequencies and cell numbers infiltrating Tollip-deficient adenomas compared with WT (Figure 5F). Conversely, no differences in Treg frequency or cell number were noted in other lymphoid organs (Figure S5C). Altogether, our data show that Tollip deficiency leads to reduced $CD3^+$ T cell accumulation in colonic adenoma together with a local imbalance between effector and regulatory T cells.

Collectively, these data suggest that decreased adenoma risk in Tollip-deficient mice is associated with impeded immune cell infiltration and attenuated inflammatory responses together with abrogated Treg infiltration.

DISCUSSION

Aberrant activation of TLR and NF-κB signaling modifies risk of colitis and cancer development in mice (Shao et al., 2013; Xiao et al., 2007; Kesselring et al., 2016; Begka et al., 2016). Tollip is an intracellular adaptor able to negatively regulate IL-1R and TLR2/TLR4-mediated NF-κB activation and to promote tolerance in intestinal epithelial cells (IECs) (Bulut et al., 2001; Burns et al., 2000; Otte et al., 2004). We hypothesized that Tollip deficiency would promote CAC risk, based on our previous findings (Maillard et al., 2014) and what had been previously reported on other innate negative regulators (Salcedo et al., 2010; Xiao et al., 2007; Begka et al., 2016). However, we observed that Tollip$^{-/-}$ mice were partially protected against CAC and that Tollip expression tended to be downregulated in dysplastic lesions from patients with UC.

Although prominent epithelial damage was observed early on the AOM/DSS regime, this only evolved to blunted tumor development characterized by reduced cell turnover. This could be in part due to a reduced number of surviving epithelial cells subjected to AOM-induced mutagenesis. Although increased epithelial apoptosis activates STAT3-mediated pro-repair and neoplastic responses (Bollrath et al., 2009), histologically we did not find any difference in STAT3 protein expression. Similarly, analysis of STAT3 activation pathway showed that it remained unchanged upon Tollip deficiency.

Following epithelial destruction and microbial incursion, infiltrating leukocytes not only support anti-microbial responses but also fuel tumorigenesis via excessive cytokine and growth factor production (Danese and Mantovani, 2010; West et al., 2015). Interestingly, Tollip deficiency led to poor leukocyte recruitment to tumoral tissues despite prominent epithelial disruption at early stages of acute DSS-induced injury. Our findings correlate with prior reports on TLR4 signaling, in which Tollip actively participates. Indeed, TLR4 deficiency promoted colitis induction but attenuated tumor development and growth due to reduced leukocyte infiltration into inflamed mucosa (Fukata et al., 2005, 2007).

Consistently, Diao and colleagues reported decreased numbers of Ly-6G^{+} cells infiltrating the colonic mucosa of Tollip$^{-/-}$ mice upon acute colitis. In addition, Tollip-deficient CCR5^{+} neutrophils accumulated in the blood due to decreased chemotactic receptor FPR2 levels, indicating defective migration of these cells into inflamed colonic mucosal sites (Diao et al., 2016). CCR5 is an inflammatory chemokine receptor enabling recruitment of diverse immune cell types (Griffith et al., 2014). In a phase I clinical trial of metastatic colorectal cancer, drug-induced blockade of CCR5+CD4^{+} and CD8^{+} lymphocyte infiltration with maraviroc reduced interaction of lymphocytes with MΦs, leading to reduced inflammation and better clinical responses (Halama et al., 2016). Ablation of chemokine receptors, such as CCR2 and CXCR2, was shown to severely abrogate leukocyte infiltration, resulting in reduced inflammation-driven colon cancer (Popivanova et al., 2008, 2009; Katoh et al., 2013). Notably, we demonstrated a pronounced decrease in *Ccr5* expression in the colonic mucosa of unchallenged Tollip $^{-/-}$ mice, indicating a potential correlation between Tollip-Ccr5 expression and modulation of leukocytes trafficking, which deserves further study.

Tollip ablation influenced not only chemokine receptors expression but also lymphocyte homing molecules causing altered T cells migratory patterns. As such, a pronounced *Cd62l* mRNA decrease in colonic mucosa correlated with increased accumulation of naive CD8^{+} CD62L^{+} T cells in the blood of Tollip$^{-/-}$ unchallenged mice. This effect was even more pronounced in Tollip-deficient adenomas, where we observed a prominent reduction in CD3^{+} T lymphocyte infiltrates. This colon-specific reduction was restricted to colorectal carcinogenesis, as it could not be detected in peripheral lymphoid organs or upon homeostatic conditions. Remarkably, decreased CD3^{+} T lymphocyte infiltration was mainly due to reduced CD4^{+} Foxp3^{+} Treg cells recruitment in the tumor microenvironment. In line with this observation, we observed a significant decrease in *Ctla4* mRNA expression in Tollip-deficient adenomas, a receptor expressed on Treg cells. Finally, defects in TGFβR signaling activation further argued for reduced immune-suppressive responses in tumor microenvironment upon Tollip ablation. We suggest that, already during homeostasis, Tollip ablation predisposes leukocytes accumulation in the periphery. In addition, Tollip deficiency also affects leukocyte recruitment, predominantly Treg cells, to adenomatous lesions.

Although Treg cells are key factors of intestinal homeostasis and protect against colitis (Mottet et al., 2003; Tanoue et al., 2016), their role in colitis-induced cancer was recently associated with poor prognosis (Pastille et al., 2014). As such, depletion of Tregs during acute CAC resulted in increased intestinal inflammation, whereas ablation of Tregs at late CAC state promoted CD8^{+}-induced IFNγ/granzyme

B antitumoral responses, resulting in hindered tumor progress (Pastille et al., 2014). Hence, our observations support the concept that reduced Treg infiltration upon Tollip ablation into the inflamed colonic mucosa might underlie early CAC events by facilitating epithelial destruction, whereas attenuated cell infiltration, due to Tollip ablation, on late CAC phase seems to play a protective role, resulting in reduced immune suppressive responses and partial protection from CAC onset and development.

The exact molecular mechanisms through which Tollip may alter leukocytes migratory capacity remains unknown. Several studies have shown that Tollip promotes endosomal trafficking of receptors for either lysosomal degradation or nuclear translocation (Brissoni et al., 2006; Zhu et al., 2012; Ciarrocchi et al., 2009). As such, Tollip deficiency resulted in impaired trafficking and accumulation of IL-1R in late endosomes (Brissoni et al., 2006). Therefore, we hypothesize that Tollip deficiency may impair endosomal trafficking of several chemokine receptors and T cell homing factors, such as CCR5 and CD62L.

Altogether, our human and murine data indicate that Tollip plays a dual role in being protective against colitis while exacerbating colitis-induced cancer in mice. Our findings implicate Tollip in the expression of several homing/trafficking molecules of relevance to anti-tumoral immunity, including T lymphocytes and Treg subset infiltration. Thus, shifts in anti-tumoral immunity profile together with defects in TGFβR signaling underlie partial protection from colitis-associated cancer. Future studies should assess the role of Tollip in the turnover of inflammatory and suppressive receptors, as well as in leukocyte migration to inflammatory and cancerous sites.

Limitations of the Study

Our initial findings using human samples were only exploratory due to limited sample size. This was in part due to the rare incidence of colitis-associated cancer in human subjects and also to a limited number of patients screened in the GETAID cohort. In addition, samples obtained from the SIBDCS were only taken in active versus inactively inflamed colon segments prompting us to complete our dataset with samples coming from different sources.

To explore the mechanisms underlying colitis-associated cancer development, we employed the widely accepted and established AOM/DSS mouse model. Although this model is thought to most closely reflect human CAC development, kinetics of adenoma development is more rapid in mice than in humans, putting some limitations in the analyses of cell-recruitment dynamics in tumors. Moreover, AOM/DSS-treated mice mostly develop non-invasive adenomas, whereas in humans the carcinogenic process may evolve to a fully blown invasive adenocarcinoma. As Tollip expression may be different between low-grade and advanced adenomas, more detailed analyses could not be done in the mouse setting.

METHODS

All methods can be found in the accompanying Transparent Methods supplemental file.

CONSORTIA

Members of the SIBDCS Study Group

Claudia Anderegg, Peter Bauerfeind, Christoph Beglinger, Stefan Begré, Dominique Belli, José M. Bengoa, Luc Biedermann, Beat Bigler, Janek Binek, Mirjam Blattmann, Stephan Boehm, Jan Borovicka, Christian P. Braegger, Nora Brunner, Patrick Bühr, Bernard Burnand, Emanuel Burri, Sophie Buyse, Matthias Cremer, Dominique H. Criblez, Philippe de Saussure, Lukas Degen, Joakim Delarive, Christopher Doerig, Barbara Dora, Gian Dorta, Mara Egger, Tobias Ehmann, Ali El-Wafa, Matthias Engelmann, Jessica Ezri, Christian Felley, Markus Fliegner, Nicolas Fournier, Montserrat Fraga, Pascal Frei, Remus Frei, Michael Fried, Florian Froehlich, Christian Funk, Raoul Ivano Furlano, Suzanne Gallot-Lavallée, Martin Geyer, Marc Girardin, Delphine Golay, Tanja Grandinetti, Beat Gysi, Horst Haack, Johannes Haarer, Beat Helbling, Peter Hengstler, Denise Herzog, Cyrill Hess, Klaas Heyland, Thomas Hinterleitner, Philippe Hiroz, Claudia Hirschi, Petr Hruz, Rika Iwata, Res Jost, Pascal Juillerat, Céline Keller, Christina Knellwolf, Christoph Knoblauch, Henrik Köhler, Rebekka Koller, Claudia Krieger-Grübel, Gerd Kullak-Ublick, Patrizia Künzler, Markus Landolt, Rupprecht Lange, Frank Serge Lehmann, Andrew Macpherson, Philippe Maerten, Michel H. Maillard, Christine Manser, Michael Manz, Urs Marbet, George Marx, Christoph Matter, Rémy Meier, Martina Mendanova, Pierre Michetti, Benjamin Misselwitz, Bernhard Morell, Patrick Mosler, Christian Mottet, Christoph Müller, Pascal Müller, Beat Müllhaupt, Claudia Münger-Beyeler, Leilla Musso, Andreas Nagy, Michaela Neagu, Cristina

Nichita, Jan Niess, Andreas Nydegger, Nicole Obialo, Carl Oneta, Cassandra Oropesa, Ueli Peter, Daniel Peternac, Laetitia Marie Petit, Franziska Piccoli-Gfeller, Julia Beatrice Pilz, Valérie Pittet, Nadia Raschle, Ronald Rentsch, Sophie Restellini, Jean-Pierre Richterich, Sylvia Rihs, Marc Alain Ritz, Jocelyn Roduit, Daniela Rogler, Gerhard Rogler, Jean-Benoît Rossel, Vanessa Rueger, Gaby Saner, Bernhard Sauter, Mikael Sawatzki, Michela Schäppi, Michael Scharl, Sylvie Scharl, Martin Schelling, Susanne Schibli, Hugo Schlauri, Sybille Schmid Uebelhart, Jean-François Schnegg, Alain Schoepfer, Frank Seibold, Mariam Seirafi, Gian-Marco Semadeni, David Semela, Arne Senning, Marc Sidler, Christiane Sokollik, Johannes Spalinger, Holger Spangenberger, Philippe Stadler, Michael Steuerwald, Alex Straumann, Bigna Straumann-Funk, Michael Sulz, Alexandra Suter, Joël Thorens, Sarah Tiedemann, Radu Tutuian, Stephan Vavricka, Francesco Viani, Jürg Vögtlin, Roland Von Känel, Alain Vonlaufen, Dominique Vouillamoz, Rachel Vulliamy, Jürg Wermuth, Helene Werner, Paul Wiesel, Reiner Wiest, Tina Wylie, Jonas Zeitz, Dorothee Zimmermann.

SUPPLEMENTAL INFORMATION

Supplemental Information can be found online at https://doi.org/10.1016/j.isci.2020.100891.

ACKNOWLEDGMENTS

We would like to thank Prof. Darius Moradpour, Prof. Andrew J. Macpherson, Prof. Greta Guarda, Dr Yan Pu, Dr Giorgia Rota, Dr Anh Thu Dang, Dr Mati Moyat, Dr Zoe Enderlin Vaz da Silva, Alba Rodriguez Bryant, and Lakshanie Wickramasinghe for their helpful participation and contribution to this study. This study was supported by grants from the Emma Muschamp Foundation, Switzerland; San Salvatore Foundation, Switzerland; the Novartis Foundation, Switzerland, the Swiss Society of Gastroenterology, and the Abbvie IBD award.

AUTHOR CONTRIBUTIONS

Conception and design: C.B., D.V., and M.H.M. Development of methodology: C.B., D.V., and M.H.M. Acquisition of data (analysis, acquired and managed patients): C.B., M.H.M., and S.N. Analysis and interpretation of data (statistical analysis, biostatistics): C.B., C.P., C.M., D.V., and M.H.M. Writing, review, and revision of the manuscript: C.B., C.P., C.M., K.D.M., D.V., and M.H.M. Study supervision: D.V. and M.H.M.

DECLARATION OF INTEREST

The authors declare no conflicts of interest related to this study.

Received: March 25, 2019
Revised: August 25, 2019
Accepted: February 4, 2020
Published: March 27, 2020

REFERENCES

Becker, C., Fantini, M.C., Wirtz, S., Nikolaev, A., Kiesslich, R., Lehr, H.A., Galle, P.R., and Neurath, M.F. (2005). In vivo imaging of colitis and colon cancer development in mice using high resolution chromoendoscopy. Gut *54*, 950–954.

Begka, C., Velin, D., and Maillard, M.H. (2016). Preventing overheating: tight control of gut innate immunity in health and disease. Inflamm. Bowel Dis. *22*, 1723–1736.

Bollrath, J., Phesse, T.J., von Burstin, V.A., Putoczki, T., Bennecke, M., Bateman, T., Nebelsiek, T., Lundgren-May, T., Canli, O., et al. (2009). gp130-mediated Stat3 activation in enterocytes regulates cell survival and cell-cycle progression during colitis-associated tumorigenesis. Cancer Cell *15*, 91–102.

Brissoni, B., Agostini, L., Kropf, M., Martinon, F., Swoboda, V., Lippens, S., Everett, H., Aebi, N., Janssens, S., Meylan, E., et al. (2006). Intracellular trafficking of interleukin-1 receptor I requires Tollip. Curr. Biol. *16*, 2265–2270.

Bulut, Y., Faure, E., Thomas, L., Equils, O., and Arditi, M. (2001). Cooperation of Toll-like receptor 2 and 6 for cellular activation by soluble tuberculosis factor and Borrelia burgdorferi outer surface protein A lipoprotein: role of Toll-interacting protein and IL-1 receptor signaling molecules in Toll-like receptor 2 signaling. J. Immunol. *167*, 987–994.

Burns, K., Clatworthy, J., Martin, L., Martinon, F., Plumpton, C., Maschera, B., Lewis, A., Ray, K., Tschopp, J., and Volpe, F. (2000). Tollip, a new component of the IL-1RI pathway, links IRAK to the IL-1 receptor. Nat. Cell Biol. *2*, 346–351.

Canavan, C., Abrams, K.R., and Mayberry, J. (2006). Meta-analysis: colorectal and small bowel cancer risk in patients with Crohn's disease. Aliment. Pharmacol. Ther. *23*, 1097–1104.

Ciarrocchi, A., D'Angelo, R., Cordiglieri, C., Rispoli, A., Santi, S., Riccio, M., Carone, S., Mancia, A.L., Paci, S., Cipollini, E., et al. (2009). Tollip is a mediator of protein sumoylation. PLoS One *4*, e4404.

Danese, S., and Mantovani, A. (2010). Inflammatory bowel disease and intestinal cancer: a paradigm of the Yin-Yang interplay between inflammation and cancer. Oncogene *29*, 3313–3323.

Diao, N., Zhang, Y., Chen, K., Yuan, R., Lee, C., Geng, S., Kowalski, E., Guo, W., Xiong, H., Li, M., and Li, L. (2016). Deficiency in Toll-interacting protein (Tollip) skews inflamed yet incompetent innate leukocytes in vivo during DSS-induced septic colitis. Sci. Rep. *6*, 34672.

Fernandes, P., Macsharry, J., Darby, T., Fanning, A., Shanahan, F., Houston, A., and Brint, E. (2016). Differential expression of key regulators of Toll-like receptors in ulcerative colitis and Crohn's

disease: a role for Tollip and peroxisome proliferator-activated receptor gamma? Clin. Exp. Immunol. *183*, 358–368.

Fukata, M., Chen, A., Vamadevan, A.S., Cohen, J., Breglio, K., Krishnareddy, S., Hsu, D., Xu, R., Harpaz, N., Dannenberg, A.J., et al. (2007). Toll-like receptor-4 promotes the development of colitis-associated colorectal tumors. Gastroenterology *133*, 1869–1881.

Fukata, M., Michelsen, K.S., Eri, R., Thomas, L.S., Hu, B., Lukasek, K., Nast, C.C., Lechago, J., Xu, R., Naiki, Y., et al. (2005). Toll-like receptor-4 is required for intestinal response to epithelial injury and limiting bacterial translocation in a murine model of acute colitis. Am. J. Physiol. Gastrointest. Liver Physiol. *288*, G1055–G1065.

Greten, F.R., Eckmann, L., Greten, T.F., Park, J.M., Li, Z.W., Egan, L.J., Kagnoff, M.F., and Karin, M. (2004). IKKbeta links inflammation and tumorigenesis in a mouse model of colitis-associated cancer. Cell *118*, 285–296.

Griffith, J.W., Sokol, C.L., and Luster, A.D. (2014). Chemokines and chemokine receptors: positioning cells for host defense and immunity. Annu. Rev. Immunol. *32*, 659–702.

Halama, N., Zoernig, I., Berthel, A., Kahlert, C., Klupp, F., Suarez-Carmona, M., Suetterlin, T., Brand, K., Krauss, J., Lasitschka, F., et al. (2016). Tumoral immune cell exploitation in colorectal cancer metastases can be targeted effectively by anti-CCR5 therapy in cancer patients. Cancer Cell *29*, 587–601.

Hill, R.J., Zozulya, S., Lu, Y.L., Ward, K., Gishizky, M., and Jallal, B. (2002). The lymphoid protein tyrosine phosphatase Lyp interacts with the adaptor molecule Grb2 and functions as a negative regulator of T-cell activation. Exp. Hematol. *30*, 237–244.

Ishihara, S., Aziz, M.M., Yuki, T., Kazumori, H., and Kinoshita, Y. (2009). Inflammatory bowel disease: review from the aspect of genetics. J. Gastroenterol. *44*, 1097–1108.

Katoh, H., Wang, D., Daikoku, T., Sun, H., Dey, S.K., and Dubois, R.N. (2013). CXCR2-expressing myeloid-derived suppressor cells are essential to promote colitis-associated tumorigenesis. Cancer Cell *24*, 631–644.

Kesselring, R., Glaesner, J., Hiergeist, A., Naschberger, E., Neumann, H., Brunner, S.M., Wege, A.K., Seebauer, C., Kohl, G., Merkl, S., et al. (2016). IRAK-M expression in tumor cells supports colorectal cancer progression through reduction of antimicrobial defense and stabilization of STAT3. Cancer Cell *29*, 684–696.

Kostic, A.D., Gevers, D., Pedamallu, C.S., Michaud, M., Duke, F., Earl, A.M., Ojesina, A.I., Jung, J., Bass, A.J., Tabernero, J., et al. (2012). Genomic analysis identifies association of Fusobacterium with colorectal carcinoma. Genome Res. *22*, 292–298.

Ladoire, S., Martin, F., and Ghiringhelli, F. (2011). Prognostic role of FOXP3+ regulatory T cells infiltrating human carcinomas: the paradox of colorectal cancer. Cancer Immunol. Immunother. *60*, 909–918.

Lowe, E.L., Crother, T.R., Rabizadeh, S., Hu, B., Wang, H., Chen, S., Shimada, K., Wong, M.H., Michelsen, K.S., and Arditi, M. (2010). Toll-like receptor 2 signaling protects mice from tumor development in a mouse model of colitis-induced cancer. PLoS One *5*, e13027.

Maillard, M.H., Bega, H., Uhlig, H.H., Barnich, N., Grandjean, T., Chamaillard, M., Michetti, P., and Velin, D. (2014). Toll-interacting protein modulates colitis susceptibility in mice. Inflamm. Bowel Dis. *20*, 660–670.

Masopust, D., and Schenkel, J.M. (2013). The integration of T cell migration, differentiation and function. Nat. Rev. Immunol. *13*, 309–320.

Mottet, C., Uhlig, H.H., and Powrie, F. (2003). Cutting edge: cure of colitis by CD4+CD25+ regulatory T cells. J. Immunol. *170*, 3939–3943.

Otte, J.M., Cario, E., and Podolsky, D.K. (2004). Mechanisms of cross hyporesponsiveness to Toll-like receptor bacterial ligands in intestinal epithelial cells. Gastroenterology *126*, 1054–1070.

Pastille, E., Bardini, K., Fleissner, D., Adamczyk, A., Frede, A., Wadwa, M., von Smolinski, D., Kasper, S., Sparwasser, T., Gruber, A.D., et al. (2014). Transient ablation of regulatory T cells improves antitumor immunity in colitis-associated colon cancer. Cancer Res. *74*, 4258–4269.

Pimentel-Nunes, P., Goncalves, N., Boal-Carvalho, I., Afonso, L., Lopes, P., Roncon-Albuquerque, R., Jr., Soares, J.B., Cardoso, E., Henrique, R., et al. (2012). Decreased Toll-interacting protein and peroxisome proliferator-activated receptor gamma are associated with increased expression of Toll-like receptors in colon carcinogenesis. J. Clin. Pathol. *65*, 302–308.

Popivanova, B.K., Kitamura, K., Wu, Y., Kondo, T., Kagaya, T., Kaneko, S., Oshima, M., Fujii, C., and Mukaida, N. (2008). Blocking TNF-alpha in mice reduces colorectal carcinogenesis associated with chronic colitis. J. Clin. Invest. *118*, 560–570.

Popivanova, B.K., Kostadinova, F.I., Furuichi, K., Shamekh, M.M., Kondo, T., Wada, T., Egashira, K., and Mukaida, N. (2009). Blockade of a chemokine, CCL2, reduces chronic colitis-associated carcinogenesis in mice. Cancer Res. *69*, 7884–7892.

Rakoff-Nahoum, S., and Medzhitov, R. (2007). Regulation of spontaneous intestinal tumorigenesis through the adaptor protein MyD88. Science *317*, 124–127.

Rakoff-Nahoum, S., Paglino, J., Eslami-Varzaneh, F., Edberg, S., and Medzhitov, R. (2004). Recognition of commensal microflora by toll-like receptors is required for intestinal homeostasis. Cell *118*, 229–241.

Rutter, M., Saunders, B., Wilkinson, K., Rumbles, S., Schofield, G., Kamm, M., Williams, C., Price, A., Talbot, I., and Forbes, A. (2004). Severity of inflammation is a risk factor for colorectal neoplasia in ulcerative colitis. Gastroenterology *126*, 451–459.

Salcedo, R., Worschech, A., Cardone, M., Jones, Y., Gyulai, Z., Dai, R.M., Wang, E., Ma, W., Haines, D., O'hUigin, C., et al. (2010). MyD88-mediated signaling prevents development of adenocarcinomas of the colon: role of interleukin 18. J. Exp. Med. *207*, 1625–1636.

Sansom, D.M. (2000). CD28, CTLA-4 and their ligands: who does what and to whom? Immunology *101*, 169–177.

Shao, L., Oshima, S., Duong, B., Advincula, R., Barrera, J., Malynn, B.A., and Ma, A. (2013). A20 restricts wnt signaling in intestinal epithelial cells and suppresses colon carcinogenesis. PLoS One *8*, e62223.

Tanoue, T., Atarashi, K., and Honda, K. (2016). Development and maintenance of intestinal regulatory T cells. Nat. Rev. Immunol. *16*, 295–309.

Toprak, N.U., Yagci, A., Gulluoglu, B.M., Akin, M.L., Demirkalem, P., Celenk, T., and Soyletir, G. (2006). A possible role of *Bacteroides fragilis* enterotoxin in the aetiology of colorectal cancer. Clin. Microbiol. Infect *12*, 782–786.

van de Ven, K., and Borst, J. (2015). Targeting the T-cell co-stimulatory CD27/CD70 pathway in cancer immunotherapy: rationale and potential. Immunotherapy *7*, 655–667.

van Heel, D.A., Fisher, S.A., Kirby, A., Daly, M.J., Rioux, J.D., and Lewis, C.M.; Genome Scan Meta-Analysis Group of the IBD International Genetics Consortium (2004). Inflammatory bowel disease susceptibility loci defined by genome scan meta-analysis of 1952 affected relative pairs. Hum. Mol. Genet. *13*, 763–770.

West, N.R., McCuaig, S., Franchini, F., and Powrie, F. (2015). Emerging cytokine networks in colorectal cancer. Nat. Rev. Immunol. *15*, 615–629.

Whiteside, T.L. (2012). What are regulatory T cells (Treg) regulating in cancer and why? Semin. Cancer Biol. *22*, 327–334.

Xiao, H., Gulen, M.F., Qin, J., Yao, J., Bulek, K., Kish, D., Altuntas, C.Z., Wald, D., Ma, C., Zhou, H., et al. (2007). The Toll-interleukin-1 receptor member SIGIRR regulates colonic epithelial homeostasis, inflammation, and tumorigenesis. Immunity *26*, 461–475.

Zhang, G., and Ghosh, S. (2002). Negative regulation of toll-like receptor-mediated signaling by Tollip. J. Biol. Chem. *277*, 7059–7065.

Zhu, L., Wang, L., Luo, X., Zhang, Y., Ding, Q., Jiang, X., Wang, X., Pan, Y., and Chen, Y. (2012). Tollip, an intracellular trafficking protein, is a novel modulator of the transforming growth factor-beta signaling pathway. J. Biol. Chem. *287*, 39653–39663.

iScience, Volume *23*

Supplemental Information

Toll-Interacting Protein Regulates Immune Cell Infiltration and Promotes Colitis-Associated Cancer

Christina Begka, Céline Pattaroni, Catherine Mooser, Stéphane Nancey, Swiss IBD Cohort Study Group, Kathy D. McCoy, Dominique Velin, and Michel H. Maillard

Supplementary Information

SUPPLEMENTAL FIGURES

Figure S1.

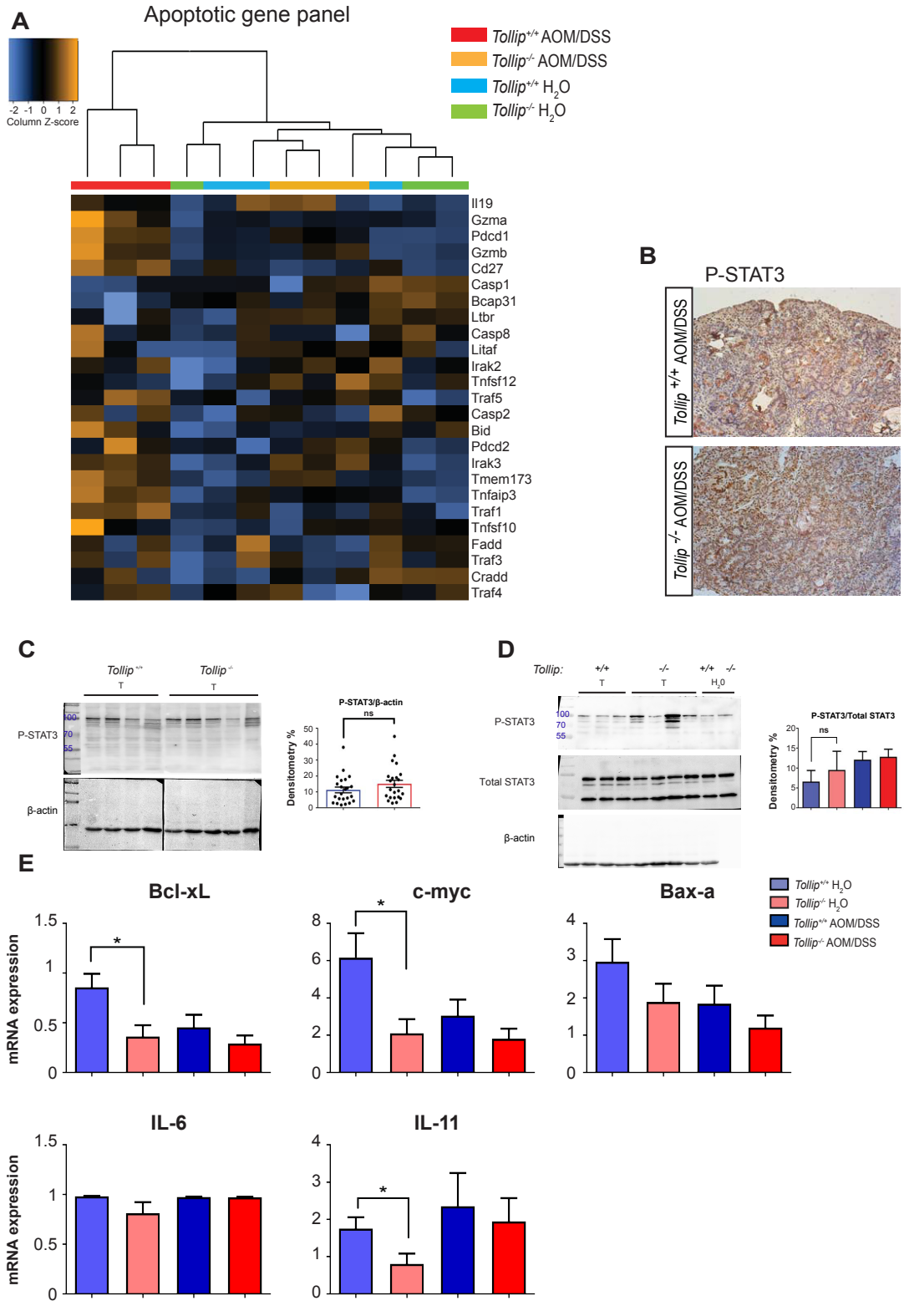

Figure S1. STAT3 pathway is functional upon Tollip deficiency. Related to Figure 3.

A. Heat map of apoptotic genes immune profiling panel for both untreated and treated Tollip$^{-/-}$ and WT mice for days 0 and 63 (data obtained from three biological replicates per group), respectively. **B.** Representative immunohistochemical P-STAT3 and nuclear staining with hematoxylin in adenomas of paraffin-embedded colons from AOM/DSS-treated Tollip$^{-/-}$ and WT mice. Scale bars: 100 μm. **C.** Immunoblot analysis for phosphorylated STAT3 (P-STAT3 2 bands at 86, 79kD) extracted from whole colon homogenates from tumors (T) of AOM/DSS-treated Tollip$^{-/-}$ and WT mice. β-actin (at 42kD) was used as a loading control. The molecular bands of 100, 70 and 55kD are noted in the pre-stained protein ladder that appears before the protein bands of interest. The same nitrocellulose membrane was used for the immunoblotting of all three markers. Relative protein expression was defined by the densitometry ratio of P-STAT3 / β-actin. Data are mean ± SEM. n= 23 adenomas. Differences were analyzed by Mann-Whitney test. ns, p=0.1612 **D.** Immunoblot analysis for P-STAT3 (2 bands at 86, 79kD) and total STAT3 (2 bands at 91 and 86kD) extracted from whole colon homogenates from tumors (T) of both treated Tollip$^{-/-}$ and WT mice or from untreated animals (H_2O group). β-actin (at 42kD) was used as a loading control. The molecular bands of 100, 70 and 55kD are noted in the pre-stained protein ladder that appears before the protein bands of interest. The same nitrocellulose membrane was used for the immunoblotting of all three markers. Relative protein expression was defined by the densitometry ratio of P-STAT3/Total STAT-3. Differences were analyzed by Mann-Whitney test. ns, p=0.8857 and p=0.5320 values were calculated for (T) groups and untreated mice, respectively. **E.** Relative mRNA expression of *Bcl-xL, c-myc, Bax-α, Il-6*, and *Il-11* were analyzed by real-time PCR. *Gadph* was used as a house keeping gene. Data are mean ± SEM. n= 5-19 samples. Differences were analyzed by two-tailed unpaired t-test. p=0.015 for *Bcl-xL*, p=0.0167 for *c-myc* and *p=0.0324* for IL-11 of colon homogenates of untreated mice. ns $p > 0.5$, *$p < 0.05$.

Figure S2.

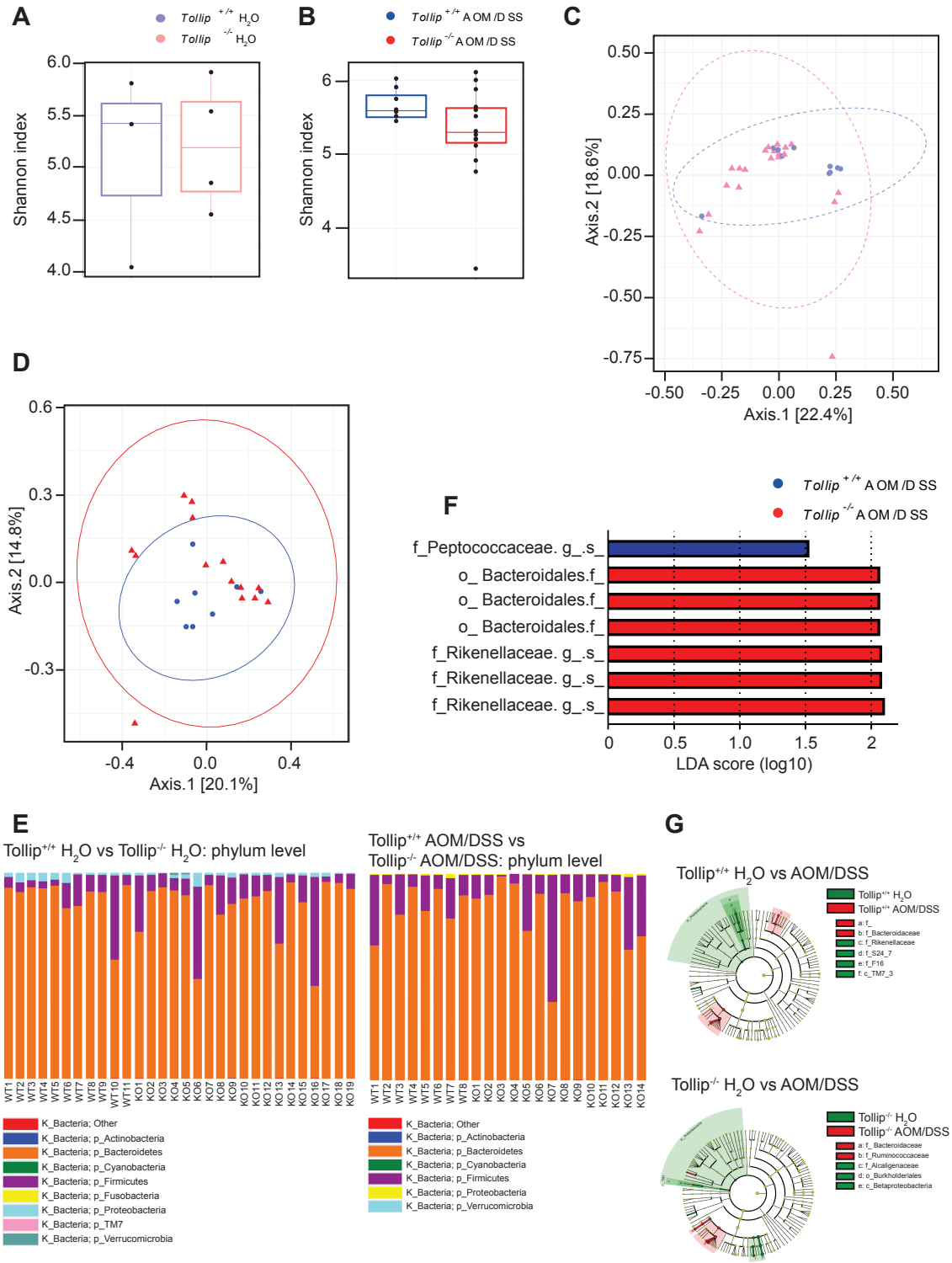
A
Tollip +/+ H2O
Tollip -/- H2O
Shannon index
6.0
5.5
5.0
4.5
4.0
B
Tollip +/+ A OM /D SS
Tollip -/- A OM /D SS
Shannon index
6
5
4
C
Axis.2 [18.6%]
0.50
0.25
0.00
-0.25
-0.50
-0.75
-0.50 -0.25 0.00 0.25 0.50
Axis.1 [22.4%]
D
Axis.2 [14.8%]
0.6
0.3
0.0
-0.3
-0.4 0.0 0.4
Axis.1 [20.1%]
F
Tollip +/+ A OM /D SS
Tollip -/- A OM /D SS
f_Peptococcaceae. g_.s_
o_ Bacteroidales.f_
o_ Bacteroidales.f_
o_ Bacteroidales.f_
f_Rikenellaceae. g_.s_
f_Rikenellaceae. g_.s_
f_Rikenellaceae. g_.s_
0 0.5 1.0 1.5 2
LDA score (log10)
E
Tollip+/+ H2O vs Tollip-/- H2O: phylum level
Tollip+/+ AOM/DSS vs
Tollip-/- AOM/DSS: phylum level
K_Bacteria; Other
K_Bacteria; p_Actinobacteria
K_Bacteria; p_Bacteroidetes
K_Bacteria; p_Cyanobacteria
K_Bacteria; p_Firmicutes
K_Bacteria; p_Fusobacteria
K_Bacteria; p_Proteobacteria
K_Bacteria; p_TM7
K_Bacteria; p_Verrucomicrobia
G
Tollip+/+ H2O vs AOM/DSS
Tollip+/+ H2O
Tollip+/+ AOM/DSS
Tollip-/- H2O vs AOM/DSS
Tollip-/- H2O
Tollip-/- AOM/DSS

Figure S2. Reduced tumor incidence in Tollip deficient mice does not correlate with altered microbiota composition and bacterial diversity. Related to Figure 2. 16S RNA analysis was performed in stool samples collected prior to AOM/DSS treatment and after CAC development (day 63) for co-housed Tollip$^{-/-}$ and WT littermate mice, respectively. **A-B.** Analysis of α-diversity was estimated by using Shannon index for stool samples of unchallenged and treated Tollip$^{-/-}$ and WT mice. Data are mean ± SEM. n= 10-20 and n= 8-14 mice, respectively. Differences were analyzed by Mann-Whitney test. **C-D.** Analysis of β diversity between stool samples of unchallenged and treated of Tollip$^{-/-}$ and WT by principal coordinates of analysis (PCoA) based on a 97% OTUs similarity with weighted Unifrac. ANOSIM p=0.474 and p=0.5083, n= 10-20 and n= 8-14 mice, for unchallenged and treated of Tollip $^{-/-}$ and WT, respectively. **E.** Evaluation of taxonomy differences in the phylum level prior and post treatment in the stool of Tollip deficient and WT littermates. **F.** Histogram of LDA scores for differentially abundant genera in stool samples between treated of Tollip$^{-/-}$ and WT mice. Blank spaces represent unclassified genera within *Bacteroidales* and *Rikenellaceae* families. **G.** Cladogram presentation of differences in L7 species level for untreated Tollip WT vs treated WT and for untreated Tollip$^{-/-}$ vs treated Tollip$^{-/-}$ mice.

Figure S3.

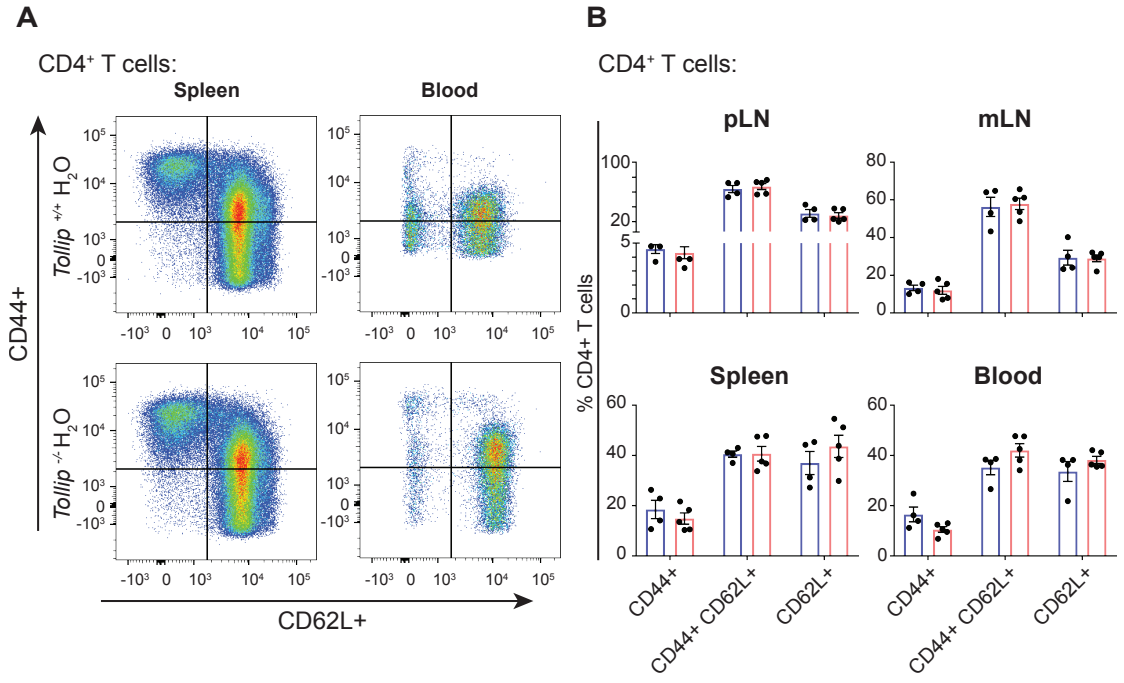

Figure S3. Unchanged CD4^{+} T lymphocytes accumulation in the periphery of Tollip deficient mice upon homoeostasis. Related to Figure 4. **A.** Representative FACS plots of CD44 CD62L pre-gated on CD4^{+} T cells from spleen homogenates and blood. **B.** Flow cytometry analysis of naïve and effector CD4^{+} T cells frequencies isolated from peripheral (pLN), mesenteric (mLN) lymph nodes, spleen and blood. Data are mean ± SEM. Differences were analyzed by Mann-Whitney test. n= 3-5 mice, ns, p>0.5.

Figure S4.

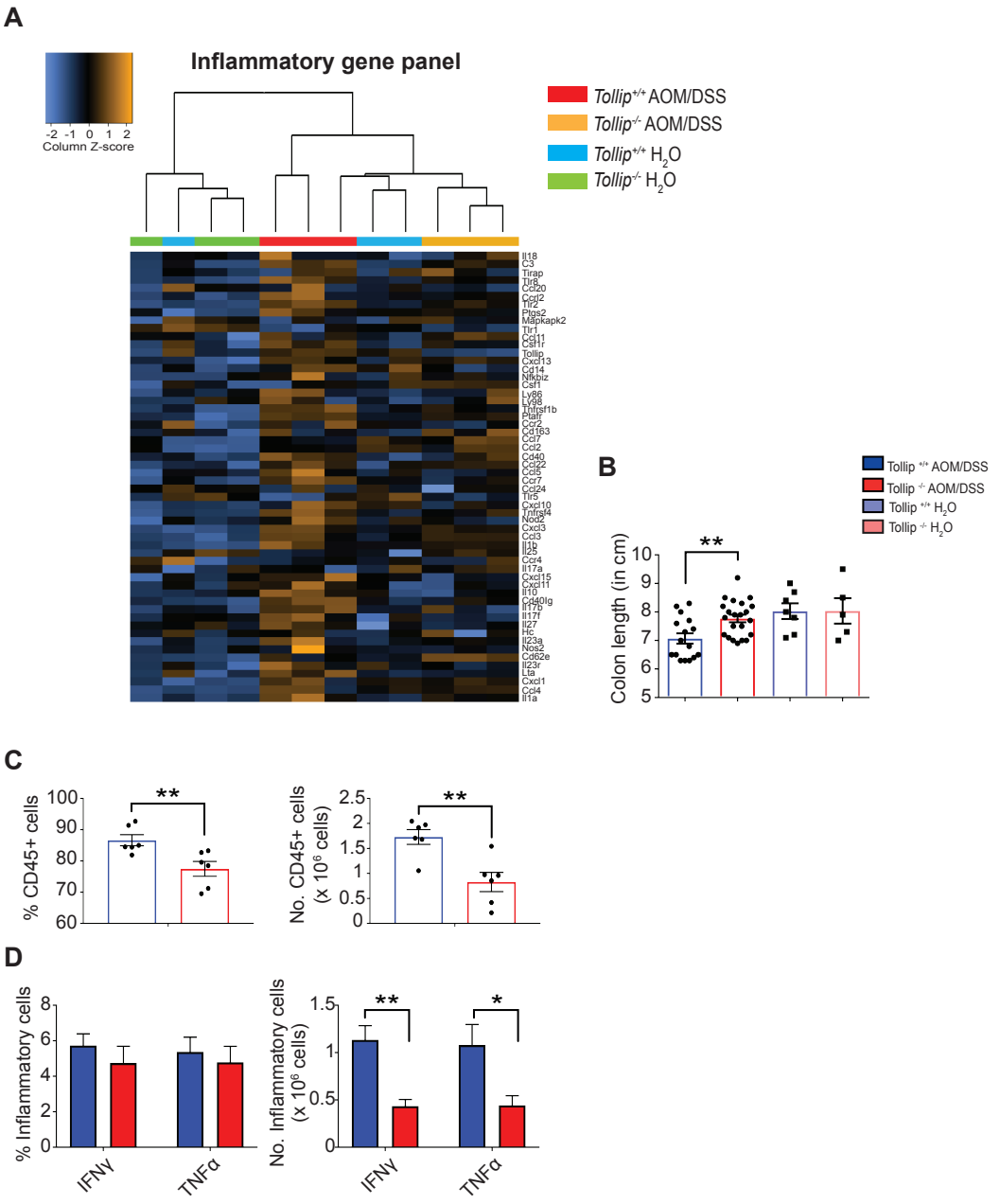

Figure S4. Tollip is required for the induction of non-resolving inflammatory responses. Related to Figure 5. A. Heat map of inflammatory genes immune profiling panel for both untreated and treated Tollip$^{-/-}$ and WT mice for days 0 and 63 (data obtained from three biological replicates per group). **B.** On day 63, colon length was evaluated for both untreated and AOM/DSS-treated Tollip$^{-/-}$ and WT mice. Data are mean ± SEM. Differences were analyzed by Mann-Whitney test, n= 5-22 mice, p=0.0013. **C.** Flow cytometry analysis of CD45^{+} cells frequencies and absolute cell number infiltrating the adenomas of Tollip$^{-/-}$ and WT mice. Data are mean ± SEM. Differences were analyzed by Mann-Whitney test, n=6 mice, p=0.0087 and p=0.0043 values were calculated for CD45^{+} frequency and absolute number

values, respectively. **D.** Flow cytometry analysis of adenoma-infiltrating CD45^{+} inflammatory cells (T and B cell lineage negative cells) cell frequency and absolute cell number that produce IFNγ and TNF in AOM/DSS-treated Tollip$^{-/-}$ and WT mice. Data are mean ± SEM. Differences were analyzed by two-way ANOVA test. n=6 mice, p=0.0060 and p=0.018 values were calculated for IFNγ^{+} and TNFα^{+} producing cells, respectively. *p < 0.05, **p < 0.01.

Figure S5.

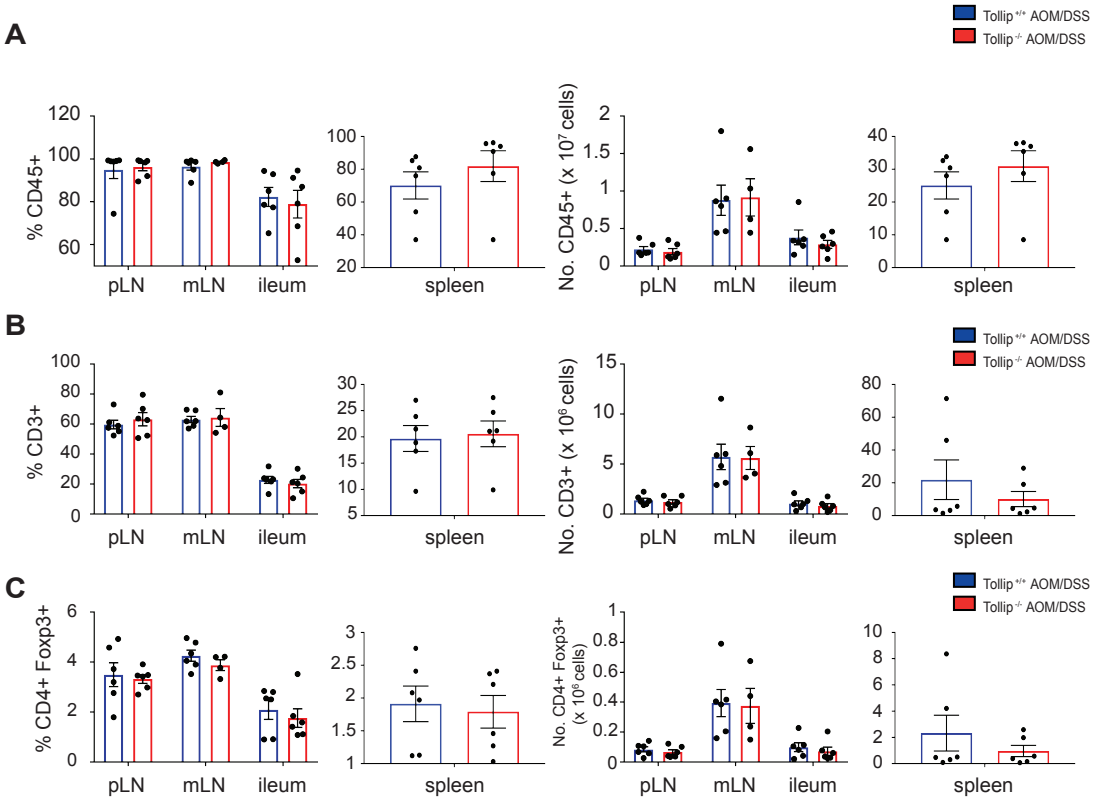

Figure S5. No alterations in leukocytes accumulation in the periphery of treated Tollip deficient mice. Related to Figure 5. A-B-C. Flow cytometry analysis of CD45^{+}, CD3^{+} T cells and T regulatory CD4^{+}Foxp3^{+} cell frequencies and absolute numbers infiltrates in peripheral (pLN) and mesenteric (mLN) lymph nodes, ileum and spleen of treated Tollip$^{-/-}$ and WT mice. Data are mean ± SEM. Differences were analyzed with Mann-Whitney test, n=6 mice, ns, p>0.5.

Table S1

Tollip-/- vs *Tollip*+/+ H2O	Log2 fold change	P-value	BH.p.value
Cd62l	-1.57	5.76E-05	0.0196
Ccr5	-0.879	8.79E-05	0.0196
Tollip	-1.2	0.000223	0.033
Ptpn22	-1.04	0.000556	0.0531
Il10ra	-0.65	0.000596	0.0531
Pax5	-1.32	0.00168	0.109
Cd44	-0.443	0.00173	0.109
Il7r	-0.972	0.00196	0.109
Itgb2	-0.403	0.00255	0.119
Mx1	-0.789	0.0028	0.119
Itga4	-0.581	0.00303	0.119
Ccr7	-0.994	0.00322	0.119
Csf2rb	-0.897	0.00467	0.154
Tlr9	-0.586	0.00488	0.154
Tnfrsf1b	-0.641	0.0052	0.154
Tnfsf14	-0.794	0.00575	0.155
Cd53	-0.76	0.00592	0.155
Btla	-0.859	0.00714	0.16
Ifi204	-0.749	0.00725	0.16
Cxcr4	-0.933	0.00734	0.16

Table S1. Related to Figure 4. Differential expression values of multi-RNA immune analysis in colon homogenates of untreated Tollip$^{-/-}$ and WT mice on day 63 (data obtained from three biological replicates per group).

Table S2

Tollip-/- vs *Tollip+/+* AOM/DSS	Log2 fold change	P-value	BH.p.value
Tollip	-1.46	5.76E-05	0.0193
Ctla4	-2.06	8.67E-05	0.0193
Cd27	-1.3	0.000156	0.0231
Ptpn22	-1.08	0.000447	0.0497
Map4k1	-0.931	0.000626	0.0557
Itgb2	-0.469	0.00102	0.0637
Cd3e	-0.843	0.00116	0.0637
Itga4	-0.676	0.00123	0.0637
Il10ra	-0.576	0.00129	0.0637
Traf1	-0.691	0.00151	0.0671
Cd19	-1.4	0.00188	0.0716
Ccr5	-0.543	0.00204	0.0716
Sh2d1a	-1.27	0.00228	0.0716
Ccl12	1.44	0.00242	0.0716
Vcam1	-0.855	0.00253	0.0716
Syk	-0.807	0.00286	0.0716
Ccr7	-1.01	0.00288	0.0716
Tlr2	-0.25	0.00305	0.0716
Btla	-0.989	0.00332	0.0716
Il27ra	-0.832	0.00334	0.0716

Table S2. Related to Figure 5. Differential expression values of multi-RNA immune analysis in colon homogenates of AOM/DSS-treated Tollip$^{-/-}$ and WT mice on day 63 (data obtained from three biological replicates per group).

Transparent Methods

KEY RESOURCES TABLE

REAGENT or RESOURCE	SOURCE	IDENTIFIER
Antibodies		
Rat Anti-Mouse CD45 Monoclonal Antibody, Biotin Conjugated, clone 30-F11	BD Biosciences	Cat# 553078, RRID:AB_394608
Armenian Hamster Anti-Mouse CD3e, Monoclonal Antibody, PE-Cyanine5 Conjugated, clone 145-2C11	BD Biosciences	Cat# 553065, RRID:AB_394598
Rat Anti-Mouse CD19 Monoclonal Antibody, FITC Conjugated, Clone 1D3	BD Biosciences	Cat# 553785, RRID:AB_395049
Rat Anti-Mouse CD25, Monoclonal Antibody, Phycoerythrin Conjugated, Clone PC61	BD Biosciences	Cat# 553866, RRID:AB_395101
Rat Anti-Mouse CD11b Monoclonal Antibody, PerCP-Cy5.5 Conjugated, Clone M1/70	BD Biosciences	Cat# 561114, RRID:AB_2033995
Rat Anti-Mouse Ly-6C Monoclonal Antibody, FITC Conjugated, Clone AL-21	BD Biosciences	Cat# 553104, RRID:AB_394628
Rat Anti-Mouse Ly-6G Monoclonal Antibody, Phycoerythrin Conjugated, Clone 1A8	BD Biosciences	Cat# 551461, RRID:AB_394208
Rat Anti-Mouse Ly-6G, Ly-6C Monoclonal Antibody, Biotin Conjugated, Clone RB6-8C5	BD Biosciences	Cat# 553124, RRID:AB_394640
Rat Anti-Mouse IFN-gamma Monoclonal Antibody, FITC Conjugated, Clone XMG1.2	BD Biosciences	Cat# 554411, RRID:AB_39537
Rat Anti-CD4, Monoclonal Antibody, FITC Conjugated, Clone RM4-5	BD Biosciences	Cat# 553046, RRID:AB_394582
Rat Anti-Mouse IL-17A, Monoclonal Antibody, FITC Conjugated, Clone TC11-18H10	BioLegend	Cat# 506907, RRID:AB_536009
Rat Anti-mouse CD45, Monoclonal antibody, Alexa Fluor® 700 Conjugated, Clone 30-F11	BioLegend	Cat# 103127, RRID:AB_493714
Mouse Anti-mouse CD45.2, Monoclonal antibody, APC/Cyanine7 Conjugated, Clone 104	BioLegend	Cat# 109824, RRID:AB_830789
Rat Anti-mouse CD3, Monoclonal antibody, Alexa Fluor® 700 Conjugated, Clone 17A2	BioLegend	Cat# 100216, RRID:AB_493697
Rat Anti-mouse CD8a, Monoclonal antibody, APC Conjugated, Clone 53-6.7	BioLegend	Cat# 100712, RRID:AB_312751
Rat Anti-mouse CD4, Monoclonal antibody, Pe/Cyanine7 Conjugated, Clone GK1.5	BioLegend	Cat# 100421, RRID:AB_312706

Mouse anti-human CD4, Monoclonal antibody, APC/Cyanine7 Conjugated, Clone RPA-T4	BioLegend	Cat# 300517, RRID:AB_314085
Armenian Hamster Anti-mouse CD11c, Monoclonal Antibody, APC Conjugated, Clone N418	BioLegend	Cat# 117310, RRID:AB_313779
Rat anti-mouse Ly-6G/Ly-6C (Gr-1), Monoclonal antibody, Pe/Cyanine7 Conjugated, Clone RB6-8C5	BioLegend	Cat# 108416, RRID:AB_313381
Rat anti-mouse F4/80, Monoclonal antibody, Pe/Cyanine7 Conjugated, Clone BM8	BioLegend	Cat# 123114, RRID:AB_893478
Armenian Hamster Anti-mouse CD103, Monoclonal Antibody, Phycoerythrin Conjugated, Clone 2E7	BioLegend	Cat# 121406, RRID:AB_1133989
Rat Anti-mouse TNF-alpha, Monoclonal antibody, Pe/Cyanine7 Conjugated, Clone MP6-XT22	BioLegend	Cat# 506324, RRID:AB_2256076
Rat Anti-Mouse FOXP3 Monoclonal Antibody, PE-Cyanine7 Conjugated, Clone FJK-16s	eBiosciences, Thermo Fisher Scientific	Cat# 25-5773-80, RRID:AB_891554
Rat Anti-Mouse IL-22 Monoclonal Antibody, Phycoerythrin, Clone 1H8PWSR	eBiosciences, Thermo Fisher Scientific	Cat# 12-7221-82, RRID:AB_10597428
Streptavidin PE-Cy5 100 ug antibody	Thermo Fisher Scientific	Cat# 15-4317-82, RRID:AB_10116415
Ki67 antibody-Proliferation Marker, Clone SP6	Abcam	Cat# ab16667, RRID:AB_302459
p53 Protein, monoclonal antibody, Unconjugated, Clone IMX25	Vector Laboratories	Cat# VP-P952, RRID:AB_2336629
Mouse Anti-Mouse Phospho-p53 (Ser15), monoclonal antibody, Clone 16G8	Cell Signaling Technology	Cat# 9286, RRID:AB_331741
Rabbit Anti-Phospho-Smad2 (Ser465/467) Antibody	Cell Signaling Technology	Cat# 3101, RRID:AB_331673
Phospho-Smad2 (Ser465/467) (138D4) Rabbit mAb antibody	Cell Signaling Technology	Cat# 3108, RRID:AB_490941
Phospho-Stat3 (Tyr705) (D3A7) XP Rabbit mAb antibody	Cell Signaling Technology	Cat# 9145, RRID:AB_2491009
Smad2 (D43B4) XP Rabbit mAb antibody	Cell Signaling Technology	Cat# 5339, RRID:AB_10626777
Stat3 (C-20) antibody	Santa Cruz Biotechnology	Cat# sc-482, RRID:AB_63244
Mouse Anti-Tubulin II, beta Monoclonal Antibody, Unconjugated, Clone 7B	Sigma-Aldrich	Cat# T8453, RRID:AB_1841224

Biological Samples		
Human inflammatory bowel disease (IBD) mucosal samples	Bouhnik et al., Gut 2018	Groupe d'Etudes et de Thérapeutiques des Affections Inflammatoires du tube Digestif (GETAID)
Human colitis-associated cancer (CAC) samples	Bouhnik et al., Gut 2018	Groupe d'Etudes et de Thérapeutiques des Affections Inflammatoires du tube Digestif (GETAID)
Human sporadic colorectal cancer (CRC) samples	This paper	Lausanne Institutional Biobank (BIL)/Biobank of Lausanne (BbdL)
Human healthy colon mucosa samples (adjacent to CRC samples)	This paper	Lausanne Institutional Biobank (BIL)/Biobank of Lausanne (BbdL)
Chemicals, Peptides, and Recombinant Proteins		
Azoxymethane (AOM)	Sigma-Aldrich	A5486
Dextran sulfate sodium	TdB Consultancy	9011-18-1
Antibody diluent for IHC	BD Pharmingen	559148
Liberase TL research grade	Roche	Cat# 5401020001
Dnase I	Invitrogen, Thermo Fisher Scientific	Cat# 18047-019
10X RBC Lysis Buffer	eBiosciences, Thermo Fisher Scientific	Cat# 4300-54
Live/Dead Fixable Aqua Dead Cell Stain Kit	Thermo Fisher Scientific	L34966
Complete Protease Inhibitor Cocktail	Roche	11697498001
PhosphoSTOP – Phosphatase Inhibitor Cocktail Tablets	Roche	4906837001
WesternBright ECL HRP substrate	Advansta	K-12045-D20
PrimeScriptTM RT Reagent Kit	Takara	RR037A
iQ SYBR Green Supermix	Bio-Rad	1708882

Platinum Taq DNA Polymerase	Invitrogen, Thermo Fisher Scientific	10966034
Critical Commercial Assays		
Vectastain Elite ABC Streptavidin-HRP Kit	Vector Laboratories	PK-8200
DAB Peroxidase (HRP) Substrate Kit (with Nickel), 3,3'-diaminobenzidine	Vector Laboratories	SK-4100
DeadEnd Fluorometric TUNEL System	Promega	G3250
Foxp3 / Transcription Factor Staining Buffer Set	eBiosciences, Invitrogen	Cat# 5523-00
QIAquick PCR Purification Kit	Qiagen	28104
pGEM T Easy Vector System I	Promega	A1360
Qiamp Fast DNA Stool Mini Kit	Qiagen	51604
Ion PGMTM Hi-QTM View OT2 400 kit	Thermo Fisher Scientific	A29900
Deposited Data		
Mouse (Tollip) Immune Profiling Panel (NS_Immunology_MM_C2269)	data.mendeley.com	https://data.mendeley.com/datasets/n3k75bfy5j/1
Tollip gut microbiome analysis	This paper	Available upon request
Experimental Models: Organisms/Strains		
Mouse: C57BL/6J	The Jackson Laboratory	JAX: 000664
Mouse: Tollip-/-	Dr. Kimberly Burns	Institut de Biochimie, Epalinges, Switzerland
Oligonucleotides		
Primers for qRT-qPCR: mouse *Gapdh*	Microsynth	Forward: 5'-TCA CCACCACCATGG AGAAGG-3' and reverse: 5'-GCTAAGCAGTTGG TG GTGCA-3'
Primer for qRT-qPCR: mouse *Foxp3*	Qiagen	QT00138369

Primers for qRT-qPCR: mouse *Tgf-b*	Microsynth	Forward: 5'-GGTTCATGTCATGGATGGTGC-3' and reverse: 5'-TGACGTCACTGGAGTTGTACGG-3'
Primers for qRT-qPCR: mouse *Il-10*	Microsynth	Forward: 5'-ACCTGCTCCACTGCCTTGCT-3', and reverse: 5'-GGTTGCCAAGCCTTATCGGA-3'
Primers for qRT-qPCR: mouse *Il-6*	Microsynth	Forward: 5'-CACGATTTCCCAGAGAACATGTG -3' and reverse: 5'-ACAACCACGGCCTTCCCTACTT -3'
Primer for qRT-qPCR: mouse *Il-11*	Qiagen	QT001122122
Primers for qRT-qPCR: mouse *Bcl-xl*	Microsynth	Forward: 5'-CACTGTGCGTGGAAA GCCTA-3' and reverse: 5'-AAAGTGTCCCAGCCGCC-3'
Primers for qRT-qPCR: mouse *Bax-a*	Microsynth	Forward: 5'-GTTTCATCCAGGATCGAGCAG-3' and reverse: 5'-CCCCAGTTGAAGTTGCCATC-3'
Primers for qRT-qPCR: mouse c-myc	Microsynth	Forward: 5'-TGAGCCCCTAGTGCTGCAT-3' and reverse: 5'-AGCCCGACTCCGACCTCTT-3'
Primer for qRT-qPCR: human *Gapdh*	Qiagen	QT00079247

Primers for qRT-qPCR: human *Tollip*	Microsynth	Forward: 5'-CAAGAATCCCCGCTGGAATAAG -3' and reverse: 5'-ATGGCTTTCAGGTCCTCCTCGC-3'
Software and Algorithms		
Prism 6.0	GraphPad	https://www.graphpad.com
FACS DIVA software	BD Biosciences	https://www.bdbiosciences.com
FlowJo v.10	Tree Star	https://www.flowjo.com
AxionVision Upright	Leica	https://www.leicabiosystems.com
Adobe Photoshop		https://www.adobe.com
R	R foundation for statistical	https://www.R-project.org computing
QIIME pipeline version 1.9.1	QIIME	http://qiime.org
Fusion Fx	Vilbert Lourmat, Germany	https://www.vilber.com/fusion-fx
nSolver Analysis Software 3.0 with nCounter Advanced Analysis (version 1.0.84)	Nanostring	https://www.nanostring.com/products/analysis-software
Image J	Schneider et al., 2012	https://imagej.nih.gov/ij/
ImageJ Immunoratio plugin	Tuominen et al., 2010	http://wsiserver.jilab.fi/old-jvsmicroscope-software/

Reagents and antibodies

AOM was purchased from Sigma-Aldrich and DSS (MW 47,000 Da) from TdB Consultancy, Uppsala, Sweden. For immunohistochemistry (IHC) antibody diluent was purchased from BD Pharmingen, Ki67 monoclonal antibody (SP6) from Abcam,

Streptavidin-HRP Vectastain Elite ABC Kit and DAB purchased from Vector laboratories and DeadEnd Fluorometric TUNEL System purchased from Promega. The antibodies used for western blot: total p53 (IMX25) from Vector laboratories, p-p53 (16G8), p-Smad2 (S465/476) (138D4), p-Stat3 (Tyr705) (D3A7) from Cell Signaling, USA, total Smad2 (D43B4) and total Stat3 (C20) from Santa Cruz and tubulin was purchased from Sigma. Protease and PhosphoStop inhibitors were purchased from Roche and WesternBright ECL HRP substrate from Advansta. For RNA extraction RNeasy Plus Mini Kit was purchased from Qiagen and for RT-qPCR PrimeScriptTM RT Reagent Kit was purchased from Takara Bio Inc. and iQ SYBR Green Supermix was purchased from Bio-Rad. Primers for *Foxp3*, *TGFβ*, *Il10* and *Gapdh* were all purchased from Microsynth and human *Tollip* and *Gapdh* were both purchased from Qiagen. For flow cytometry the following antibodies: CD45-biotinylated (30-F11), CD3-Pe-Cy5 (145-2C11), CD19-FITC (1D3), CD25-PE (PC61), CD11b-PerCy5.5 (M1/70), Ly-6C-FITC (AL-21), Ly-6G-PE (1A8), Gr-1 biotinylated (RB6-8C5), Foxp3-Pe-Cy7 (FJK-16s), IFNγ-FITC (XMG1.2), IL-22-PE (1H8PWSR), IL-17-FITC (TC11-18H10.1), IL-17-PE (TC11-18H10), Streptavidin PE-Cy5 (2.4G2) were all purchased from BD Biosciences and CD45-Al700 (30-F11), CD45.2-APC-Cy7 (104), CD3-Al700 (17A2), CD8a-APC (53-6.7), CD4-Pe-Cy7 (GK1.5), CD4-APC-Cy7 (RPA-T4), CD11c-APC (N418), Gr-1 Pe-Cy7 (RB6-8C5), F4-80-PE-Cy7 (BM8), CD103-PE (2E7), TNFα-PE-Cy7 (MP6-XT22) were all purchased from Biolegend and CD4-FITC (RM4-5) was purchased from Invitrogen. Foxp3 Transcription Factor Fixation/Permeabilization Concentrate and Diluent was purchased from eBioscience. For isolation of immune cells from lamina propria Liberase TL was purchased from Roche and DNase I purchased from Invitrogen. RBC lysis buffer purchased from eBioscience. See Key Resources Table for more details.

Human study subjects

This study protocol was conducted according to the ethical guidelines expressed in the Declaration of Helsiki and all including procedures were approved by the ethics committee of “Unité de Valorisation des données et des échanitllons biologiques” (VDE) of CHUV, the Lausanne Institutional Biobank (BIL) and the Biobank of Lausanne (BbdL) and the Groupe d’Etudes et de Thérapeutiques des Affections Inflammatoires du tube Digestif (GETAID) from Lyon Sud Hospital in France. All patients included in this study gave written informed consent. Biopsy specimens were taken during endoscopic examination and tumor resected tissues were obtained from surgery. IBD group included biopsies obtained from: 14 non-inflamed and 8 inflamed mucosa of active and quiescent ulcerative colitis (UC) patients, 15 non-inflamed and 10 inflamed mucosae from quiescent and active Crohn’s disease (CD) patients, respectively. Tumor groups included biopsies obtained from: 6 CAC patients, 10 normal adjacent mucosae and 10 CRC tumors paired match biopsies. Normal adjacent mucosa biopsies were used in our analysis as a control group upon comparison with the other groups.

Induction of colitis-associated cancer (CAC)

All animal experiments were approved by the Committee on Animal Experimentation of University of Lausanne and performed in compliance with the Swiss Guidelines for the Care and Use of Laboratory Animals. Pathogen-free 12-18-week-old males and females Tollip$^{-/-}$ mice and Tollip$^{+/+}$ C57BL/6 littermates were co-housed under specific pathogen-free conditions with free access to food and water during the experiments. Tollip$^{-/-}$ mice were generated by Dr Kimberly Burns (Institut de Biochimie, Epalinges, Switzerland). Mice were injected intraperitoneally (i.p.) with a single dose of 10mg/kg of the colonotropic procarcinogen azoxymethane (AOM) (Sigma) dissolved in physiological saline. This was followed by 2.5% (wt/vol) dextran sodium sulfate (DSS) (MW 47,000 Da, TdB Consultancy, Uppsala, Sweden) oral treatment in the drinking water ad libitum. Mice were allowed to drink for seven days, followed by two weeks of regular water. This cycle was repeated twice (four days of 2.5% DSS for the second and third cycle). Mice were weighted and clinically monitored every other day. Development of adenomatous lesions was monitored by mouse colonoscopy at the end of the third cycle. After colonoscopy, mice were sacrificed and colons were excised for colonic length determination, macroscopic assessment of tumor numbers and size with the use of a dissection microscope (Leica model). Resected colons were used for histological analysis, mRNA and protein analysis or for examining profiles of immune cells by flow cytometry.

Mouse endoscopic system

Development of adenomatous polyps was monitored at the end of the third cycle of CAC model with a high resolution mouse video endoscopic system, termed Coloview. Mice were anaesthetized using intraperitoneal injection of Ketamine/Xylazine cocktail

(87.5 mg/kg Ketamine/12.5 mg/kg Xylazine). The endoscopic equipment consisted of a miniature endoscope (scope 2 mm outer diameter, company), a xenon light source and an air pump for regulating inflation of the mouse colon (all from Karl Storz, Tuttlingen, Germany). The video endoscope was viewed on a color monitor and digitally recorded.

Endoscopic score evaluation

Endoscopic tumor number was assessed by counting the tumors observed during the endoscopic procedure. Ulcers were discriminated and not included in this score. Tumor sizes were graded (Becker et al., 2005) as follows from 1 to 5: grade 1 (very small but still detectable tumor), grade 2 (tumor covering up to one eight of colonic circumference), grade 3 (tumor covering up to a quarter of colonic circumference), grade 4 (tumor covering up to half of colonic circumference) and grade 5 (tumor covering more than half of colonic circumference). The total endoscopic score was a sum of the different grades of tumors encountered per mouse.

Histo-pathological analysis

Resected mouse colon tissues were flushed with PBS 1X after mouse sacrifice. Colon tissues were fixed as “Swiss-rolls” in 4% paraformaldehyde at 4°C overnight and were paraffin-embedded. Sections of 4 µm were performed for H&E staining. Evaluation of dysplasia grades and tumor counts were performed in a blind fashion by a specialized pathologist.

Immunohistochemistry

Paraffin-embedded slides of four-micrometer were deparaffinized in xylol and rehydrated with ethanol 100 to 70%. Slides were then quenched with 3% H_2O_2 for 10

minutes and washed with PBS. Antigen retrieval for rabbit anti-Ki67 monoclonal antibody (SP6, Abcam) was performed in 10mM sodium citrate buffer, pH 6.0, with 0.1% Tween20 for 10 minutes in a pressure cooker and allowed to cool in room temperature for 20 minutes. Slides were incubated with Ki67 in IHC antibody diluent (BD Pharmingen) and incubated for one hour in room temperature. A biotinylated secondary anti-rabbit antibody (Vector laboratories) was added and incubated at room temperature for one hour. Streptavidin-HRP (Vectastain Elite ABC Kit; Vector laboratories) was added and after 30 minutes the sections were stained with DAB (Vector laboratories) and counterstained with Harris hematoxylin. Slides were immersed in increasing grades of ethanol (70-100%) followed by xylene baths. Slides were mounted with Eukit and pictures acquisition was performed with Leica microscope. Ki67 proliferation index was analyzed with Image J and the plugin Immunoratio. For the assessment of the apoptotic index, slides of 4 μm were deparaffinized as described above and the TUNEL staining was performed by using the DeadEnd Fluorometric TUNEL System (Promega) according to manufacturer's recommendations. Pictures acquisition was performed with Upright AxioVision microscope. Picture analysis and apoptotic index evaluation was performed with Photoshop.

Western Blotting Analysis

Colonic tissues were mechanically disrupted with an electric pellet pestle motor in RIPA lysis buffer supplemented with protease (Roche) and phosphatase (PhosphoStop, Roche) inhibitors. Concentration of protein lysates was calculated by using the Pierce BCA Protein Assay Kit (Thermo) according to manufacturer's recommendations to ensure equal sample loading. Protein lysates were mixed with

protein blue and denaturated at 95°C for 5 minutes. 20-30 µg of protein lysates were separated on 12% SDS-polyacrylamide gel and transferred on nitrocellulose membrane of 0.2 µm (Pall Corporation, Mexico). Membranes were blocked with 5% non-fat dry milk or 5% BSA in TBST 1X for one hour in room temperature. Membranes were then incubated overnight at 4°C with antibodies to total p53 (IMX25, Vector lab), active p-p53 (16G8, Cell Signaling), p-Smad2 (S465/467, 138D4, Cell Signaling), total Smad2 (D43B4), active p-Stat3 (Tyr705, D3A7, Cell Signaling, USA) and total Stat3 (C20) from Santa Cruz and tubulin (Sigma) was used as internal control. Incubation with peroxidase conjugated secondary donkey anti-rabbit IgG (GE Healthcare, UK) or sheep- anti-mouse IgG (Abcam) antibodies was performed for one hour in room temperature. The blotted membranes were treated with WesternBright ECL HRP substrate (Advansta, Corporation, USA) and chemiluminescent signal was revealed on Fusion Fx (Vilbert Lourmat, Germany). Band densitometry was quantified with Fusion software. See Key Resources Table for more details.

RNA extraction and Quantitative RT-PCR

Dissected colonic tissues were washed and snap frozen in liquid nitrogen. Mechanical tissue disruption was performed by using mortar and pestle, while keeping the tissues in low temperature with liquid nitrogen. Total RNA isolation was performed by using RNeasy Plus Mini Kit (Qiagen, Valencia, CA) according to manufacturer's recommendations. RNA concentration and purity were determined spectophotometrically with the NanoDrop machine (ND-1000, Thermo Scientific). One microgram of total RNA was reversed transcribed into cDNA using PrimeScriptTM RT Reagent Kit (Takara Bio Inc., Otsu, JP) and oligo-dT random primers according to manufacturer's protocol. PCR amplification was performed on a MyiQ iCycler (Bio-

Rad, Hercules, CA) using 96-well microtiter plates. The PCR reaction was performed by using the iQ SYBR Green Supermix (Bio-Rad) in duplicates for each sample. PCR program included: heating of samples on 95°C for 3 minutes followed by 35 cycles of denaturating, primer annealing and extension for 60 seconds. Amplification was performed for primers specific for mouse *Foxp3*, *TGFβ*, *Il10* and *Gapdh* (all from Microsynth) and human *Tollip* and *Gapdh* (both from Qiagen). Melting curves of the amplified products were used to identify the amplicon. Quantification of messenger RNA (mRNA) for each sample was determined by using the standard curve method. For constructing the standard DNA curve, amplicons generated for the primers mentioned above by RT-PCR were purified on silica columns (QiAquick PCR purification, Qiagen) and cloned into pGEM-Teasy (Promega Corp, Madison, WI). DH5a-competent cells were used for transforming the ligated fragments and plasmid DNA was prepared using silica cartridges (Qiagen). The sequence of the cloned amplicons was determined by cycle sequencing. The concentration and purity of DNA plasmids were determined spectophotometrically with the NanoDrop machine (ND-1000, Thermo Scientific). Copy numbers were calculated using the following formula: 1 µg 1000-bp DNA = 9.1 * 10^{11} molecules. For each PCR run in the same 96-well microtiter plate, serial 10-fold dilution from 10^7 to 10^2 of the DNA plasmid were used as standard curve together with the unknown samples. The calculated number of mRNA copies for the gene of interest was then normalized per million of mRNA copies obtained for *Gapdh*, which was used as a house keeping gene. See Key Resources Table for more details.

Isolation of intestinal/ tumor-infiltrating immune cells

Excised colons were open longitudinally and washed with ice cold PBS. Tissues were cut into 2cm pieces and incubated for 20 minutes at 37°C in calcium- and magnesium-

free DMEM (Gibco) supplemented with 10 mM EDTA with gentle agitation (80 rpm). At the end of incubation tissues were washed with calcium-free PBS until obtaining a clear supernatant devoid of epithelial cells. Tissues were then cut into smaller pieces of 1 mm and incubated with the digestion mix of Liberase TL (1 Wünsch unil / ml; Roche), DNase I (1 U / ml; Invitrogen) and 2% of FBS for 20 min at 37°C under gentle agitation (80 rpm). After incubation, the supernatants were harvested in 5 ml of DMEM complemented with 10 % FBS, while fresh digestion mix was added into the undigested gut fragments. This step was performed three times for a total time of 60 minutes. At the end of the cycle the cellular suspension was centrifuge and washed twice in DMEM and filtered through a 100 µm cell strainer for eliminating any remaining debris. The cellular suspension was centrifuged and washed two more times in DMEM and filtered through a 40 µm cell strainer. After centrifugation, cells were re-suspended in ice cold PBS containing of 2% FBS and 2 mM EDTA until preceding staining with fluorescent antibodies.

Isolation of immune cells from peripheral organs

Dissection of peripheral lymph nodes (pLNs), including inguinal, axillary and brachial, mesenteric lymph nodes (mLNs) and spleen was performed. Blood was also collected from the animals. Organs were mechanically smashed and homogenized with a plastic syringe plunger. The red blood cells (RBCs) in blood and spleens were lysed with RBC lysis buffer (eBioscience), following an incubation for 10 minutes. Cell suspension was washed with PBS, centrifuged and incubation was repeated until the supernatant was devoid of RBCs. The cellular suspensions were centrifuged and washed twice in DMEM and filtered through a 40 µm cell strainer. After centrifugation, cells were re-

suspended in ice cold PBS containing of 2% FBS and 2 mM EDTA until preceding staining with fluorescent antibodies.

Flow cytometry analysis

Cells from colon, adenomas, spleen, blood, pLNs and mLNs were re-suspended in ice cold PBS containing of 2% FBS and 2 mM EDTA and incubated with Fc blockers (2.4G2, BD, San Jose, CA) for 30 minutes. This was followed by one hour incubation with the appropriate combination of antibodies, as mentioned in Key Resources Table, in ice cold PBS containing of 2% FBS and 2 mM EDTA. For estimating the population of T regulatory cells the Foxp3 Transcription Factor Fixation/Permeabilization Concentrate and Diluent Kit (eBioscience) was used according to manufacturer's protocol, followed by one hour incubation with the Foxp3-Pe-Cy7 (FJK-16s) antibody. For evaluating cytokines production, cells were stimulated for 4 hours with 10 ng / ml PMA and 1 µg / ml Ionomycin (both from Sigma-Aldrich) in the presence of 5 µg / ml protein transport inhibitor containing Brefeldin A (Golgi Plug, BD Biosciences). After staining with antibodies of cell surface markers, cells were incubated and fixed for 20 minutes with BD Cytofix/Cytoperm Fixation and Permeabilization Solution (BD Biosciences), followed by washing with PBS and 1 hour incubation with cytokine-specific intracellular antibodies, as mentioned in Key Resources Table. Dead cells were labeled with Live/Dead Fixable Aqua Dead Cell Stain Kit, as recommended by the protocol. Cells were analyzed by flow cytometry on a Fortessa X-20 flow cytometer instrument using FACS DIVA software (both from BD Biosciences). Data analysis was performed using FlowJo version 10 software (FLOWJO LLC, Ashland, OR).

Mouse Immune Profiling Panel with NanoString analysis

NanoString nCounter Analysis System for RNA analysis was performed by the "Genomics Technology Facility" in University of Lausanne, Unil. Prior to NanoString analysis, the quality and nucleic degradation of all samples was determined with the sensitive Fragment Analyser technique according to guidelines. Qubit Fluorometric Quantification was performed to ensure the exact quantity of 200 ng of RNA concentration per sample. Each investigated nucleic acid was targeted by a capture and a reporter probe that contain approximately 50 nucleotides that are complementary to the region of interest. Each capture probe carried a biotin-tag for immobilization and each reporter probe was labeled with a barcode of six fluorophores unique for each targeted sequence. The fluorescent barcodes were imaged and the software counted and decoded the barcodes. The CodeSet used was GX Assay, Mouse Immuno Profiling Panel (NS_Immunology_MM_C2269) including 561 genes (14 housekeeping genes) and 14 control RNA skipes.

NanoString statistical analysis

Statistical analysis was performed using nSolver Analysis Software 3.0 with nCounter Advanced Analysis (version 1.0.84). Normalization and differential expression were performed using the methods of Normalization within nSolver advanced analysis and Differential expression within nSolver advanced analysis. For Normalization within nSolver advanced analysis, normalization by geometric mean of reference (housekeeping) genes was performed. Housekeeping genes were automatically selected using geNorm algorithm (Vandesompele, 2002). 10 selected genes (out of 14 housekeeping in the panel). For the Differential expression within nSolver advanced analysis, linear regression model of sample group as predictor was used. The following comparisons were performed separately by the software, each one

using a different baseline group. For the baseline “comparisons to non-treated Tollip$^{+/+}$” the following comparisons were performed: treated Tollip$^{-/-}$ vs non-treated Tollip$^{+/+}$, non-treated Tollip$^{-/-}$ vs non-treated Tollip$^{+/+}$ and treated Tollip$^{+/+}$ vs non-treated Tollip$^{+/+}$. For the baseline “comparisons to treated Tollip$^{+/+}$” the following comparisons were performed: treated Tollip$^{-/-}$ vs treated Tollip$^{+/+}$, non-treated Tollip$^{-/-}$ vs treated Tollip$^{+/+}$. For the baseline “comparisons to non-treated Tollip$^{-/-}$” the following comparisons were performed: treated Tollip$^{-/-}$ vs non-treated Tollip$^{-/-}$. The results for all comparisons mentioned above were ordered from the most statistically significantly differentially expressed genes to the least. Gene differential expression by 'Estimated log fold-change', 95% confidence interval for the log fold change, p-value and an adjusted p-value by the Benjamini-Hochberg method (controlling for false discovery rate) were also estimated for all comparisons mentioned above.

Stool collection and microbial DNA extraction

Stool samples were collected from mice prior to AOM injection and on day 63 after CAC induction with the AOM/DSS model but prior to colonoscopy. After collection samples were immediately stored at -80°C without additives until processing. DNA extraction from samples was performed with Qiamp Fast DNA Stool Mini Kit (Qiagen) according to manufacturer’s recommendations. DNA concentration and purity were determined spectophotometrically with the NanoDrop machine (ND-1000, Thermo Scientific).

16S rDNA sequencing

The V5/V6 regions of 16S rRNA genes have been amplified by PCR using Platinum Taq DNA Polymerase (Invitrogen) and an input of 100 ng fecal DNA. The forward core primers have been modified by the addition of a PGM sequencing adaptor (in italic), a

'GT' spacer and unique barcode that allow up to 96 different barcodes: 5′-CCATCTCATCCCTGCGTGTCTCCGACTCAG BARCODEATTAGATACCCYGGT AGTCC -3′. They were used in combination with a reverse fusion primer 5′-*CCTCTCTATGGGCAGTCGGTGAT*ACG AGCTGACGACARCCATG-3′. The PCR product has a length of 350 bp including adaptor and barcode[1,2]. Cycling conditions consist of an initial denaturation at 94°C for 5 minutes followed by 35 cycles of 1 minute denaturation at 94°C, 20 seconds annealing at 46°C and 30 seconds elongation at 72°C. A final elongation step was performed at 72°C for 4 minutes. The PCR products were purified after 1% agarose gel electrophoresis using Gel Extraction Kit (Qiagen) according to manufacturer's instructions. Purity and concentration of the amplicon were determined using Qubit 3.0 Fluorometer (Thermo Fisher Scientific) prior to library preparation for sequencing on the IonTorrent PGM system (Life Technologies). Libraries were diluted according to manufacturer's instructions and processed using the Ion PGM™ Hi-Q™ View OT2 400 kit (Thermo Fischer Scientific) (for up to 400 bp libraries) and the Ion PGM™ Hi-Q™ View Sequencing kit (Thermo Fischer Scientific) for sequencing on an Ion 316™ V2 chip (Thermo Fischer Scientific)[3]. All the necessary equipment pieces belong to the Next Generation Sequencing platform of the University of Bern.

Microbiome analysis

Samples with less than 4000 reads were excluded from the analysis. Data analysis was performed using the QIIME pipeline version 1.9.1[4]. Operational taxonomic unit (OTU) were picked at a threshold of 97% similarity using usearch61_ref version v6.1.544[5] followed by taxonomy assignment using the Greengenes database (http://greengenes.secondgenome.com). Calculation of the α-diversity, weighted and unweighted UniFrac-based PCoA analysis and statistical analysis using Adonis and

Anosim were performed using the QIIME pipeline version 1.9.1[4]

Statistical Analysis

Data were presented as mean of ± SEM and distribution was analyzed with Mann-Whitney test, t-test and one-way ANOVA using Prism GraphPad (GraphPad Software, San Diego, CA), with the limit of significance set at p=0.05.

REFERENCES

Sundquist, A. et al. (2007). Bacterial flora-typing with targeted, chip-based Pyrosequencing. BMC Microbiol 7, 108–11.

Mamantopoulos, M. et al. (2017). Nlrp6- and ASC-Dependent Inflammasomes Do Not Shape the Commensal Gut Microbiota Composition. Immunity 47, 339-348.

Whiteley, A. S. et al. (2012). Microbial 16S rRNA Ion Tag and community metagenome sequencing using the Ion Torrent (PGM) Platform. Journal of Microbiological Methods 91, 80–88.

Caporaso, J. G. et al. (2010). QIIME allows analysis of high-throughput community sequencing data. Nat Meth 7, 335–336.

Edgar, R. C. (2010). Search and clustering orders of magnitude faster than BLAST. Bioinformatics 26, 2460–2461.